Received: 4 August 2022 | Revised: 29 December 2022 | Accepted: 23 January 2023

DOI: 10.1002/bit.28334

ARTICLE

BIOTECHNOLOGY AND BIOENGINEERING WILEY

A novel membrane stirrer system enables foam-free biosurfactant production

Patrick Bongartz[1] | Tobias Karmainski[2] | Moritz Meyer[1] | John Linkhorst[1] | Till Tiso[2] | Lars M. Blank[2] | Matthias Wessling[1,3]

[1]Department of Chemical Process Engineering (AVT.CVT), RWTH Aachen University, Aachen, Germany

[2]Department of Aachen Biology and Biotechnology (ABBt), iAMB - Institute of Applied Microbiology, RWTH Aachen University, Aachen, Germany

[3]DWI Leibniz-Institute for Interactive Materials, Aachen, Germany

Correspondence
Matthias Wessling, Department of Chemical Process Engineering (AVT.CVT), RWTH Aachen University, Forckenbeckstr. 51, 52074 Aachen, Germany.
Email: manuscripts.cvt@avt.rwth-aachen.de

Funding information
Simulations were performed with computing resources granted by RWTH Aachen University under project thes0610; Bundesministerium für Bildung und Forschung (BMBF, GlycoX project, Grant/Award Number: 161B0866B); Prototypes of the modules were financed by the Innovation Sprint of the RWTH Aachen Innovation by the "Excellence Start-up Center. NRW" initiative, funded by the state of North Rhine-Westphalia. The sponsor is the Ministry of Economy, Innovation, Digitization and Energy; DFG, German Research Foundation, under Germany's Excellence Strategy – Exzellenzcluster 2186 "The Fuel Science Center" ID: 390919832

Abstract

Bioreactors are the operative backbone, for example, for the production of biopharmaceuticals, biomaterials in tissue engineering, and sustainable substitutes for chemicals. Still, the Achilles' heel of bioreactors nowadays is the aeration which is based on intense stirring and gas sparging, yielding inherent drawbacks such as shear stress, foaming, and sterility concerns. We present the synergistic combination of simulations and experiments toward a membrane stirrer for the efficient bubble-free aeration of bioreactors. A digital twin of the bioreactor with an integrated membrane-module stirrer (MemStir) was developed with computational fluid dynamics (CFD) studies addressing the determination of fluid mixing, shear rates, and local oxygen concentration. Usability of the MemStir is shown in a foam-free recombinant production process of biosurfactants (rhamnolipids) from glucose with different strains of *Pseudomonas putida* KT2440 in a 3-L vessel and benchmarked against a regular aerated process. The MemStir delivered a maximal oxygen transfer rate (OTR_{max}) of 175 mmol L^{-1} h^{-1} in completely foam-free cultivations. With a high space-time yield (STY) of 118 mg_{RL} L^{-1} h^{-1} during a fed-batch fermentation, the effectiveness of the novel MemStir is demonstrated. Simulations show the generic value of the MemStir beyond biosurfactant production, for example, for animal cell cultivation.

KEYWORDS
antifoam, bubble-free, membrane, membrane aeration, *Pseudomonas putida*, rhamnolipid, stirrer

Patrick Bongartz and Tobias Karmainski contributed equally to this study and are first co-authors.

1 | INTRODUCTION

Bioreactors are the backbone of countless biological production processes for high-value products in the pharmaceutical and biotechnological industry by enabling the efficient cultivation of bacteria, fungi, and animal cells. However, despite technological advances in sensor technology, process control, and vessel material, the literature (Mandenius, 2016; Palomares & Ramírez, 2019) highlights that aeration as one of the major bioreactor design criteria has experienced little innovation since the twentieth century: The gas supply in submerged cultures is still performed by bubble dispersion and stirring. Due to this lack of innovation, conventional bioreactor types cannot combine low-stress mixing conditions with high gas entry. While stirred-tank reactors typically reach high volumetric mass transfer coefficients ($k_La = 360$ to 1080 h^{-1}) (Santos-Moreau et al., 2019), the shear force induced by the stirrer's tip as well as bubbles and their rupture, is a drawback in several processes, especially for shear-sensitive cell cultures or biosurfactant-producing microorganisms due to extensive foam formation (Chisti, 2000).

An improved method for gas exchange in a bioprocess regarding the foam formation tendency is membrane aeration. Membrane bioreactors, commonly used in water treatment, combine several advantages for the process: energy efficiency regarding the oxygen transfer (Syron & Casey, 2008), a significant total shear stress reduction (Henzler, 2000), linear process scaling by the expansion of membrane area (Cote et al., 1988; Drioli et al., 2005), and the absence of foam formation due to purely diffusive transport (Coutte et al., 2010; de Kronemberger et al., 2007). Since the work of Knazek et al. (1972), membrane oxygenators have become a possible but industrially less applied niche solution for ex situ bubble-free aeration of cell culture media (Charcosset, 2012; Frahm et al., 2009). Membrane oxygenators operate by contacting fluids (oxygen, carbon dioxide, and blood or medium) across a gas-permeable membrane (Djeljadini et al., 2021). Even though external membrane modules provide high volumetric efficiency, high flow rates are necessary to exchange the oxygen-poor medium in the bioreactor. Moreover, circulating the medium through the external loop complicates process design and operation and results in dissolved oxygen gradients. Furthermore, the external loop increases the chance of contamination (Carstensen et al., 2012). Because of the aforementioned limitations in external membrane modules and *inter alia* challenges in scalability and membrane fouling, membrane aeration was restricted to mammalian cell cultivation (Catapano et al., 2004; Chang & Furusaki, 1991; Frahm et al., 2009; Qi et al., 2003). Even though the oxygen demand per cell is higher in cell cultures, bacteria and fungi have higher growth rates (Guarino et al., 2004; Wagner et al., 2011); therefore, those cultivations mostly surpass the oxygen demand of cell cultures at a certain point. Contrary to external membrane modules, in situ membrane aeration can provide solutions for fermentations with higher oxygen demand. Furthermore, the in situ membrane aeration technique is beneficial for systems that are prone to foaming, such as biosurfactant production.

Rhamnolipids, a relevant class of biosurfactants, are mainly produced by the genus *Burkholderia* and *Pseudomonas* and belong to the class of glycolipids (Abdel-Mawgoud et al., 2010). As the wild-type producer *Pseudomonas aeruginosa* is an opportunistic human pathogen, rhamnolipid production with recombinant non-pathogenic *P. putida* KT2440 has been established (Tiso et al., 2017; Wittgens et al., 2011). Apart from the general challenges of microbial cultivation, biosurfactant-production processes are especially prone to extensive foaming. By aeration, when gas bubbles are introduced into the fermentation broth, the surface-active molecules (biosurfactants) adsorb at the gas-liquid interfaces enveloping the gas bubbles, forming an amphiphile-enriched layer that stabilizes the foam (Junker, 2007). Foaming in bioprocesses can reduce product quality and quantity (e.g., by protein denaturation [Vardar-Sukan, 1998]) as well as productivity and result in a loss of the whole-cell biocatalyst (Demling et al., 2020; Handa-Corrigan et al., 1989). In addition, the rising foam can block sterile filters, which endangers sterility and can lead to an overpressure in the reactor (Anic et al., 2018; Delvigne & Lecomte, 2010; Routledge, 2012). Foam formation in fermentation processes can be prevented by either adding antifoaming agents or employing mechanical foam breakers, among other techniques. However, antifoaming agents have been shown to often negatively affect the downstream processing, the oxygen transfer rate, and the growth of microorganisms depending on the type of antifoaming agent (Anic et al., 2018; Junker, 2007; Routledge, 2012). While mechanical foam breakers can reduce the foam by inducing shear stress, these instruments can have a considerable additional energy demand, thus lowering process efficiency (Brown et al., 2001). Besides using antifoaming agents or mechanical foam breakers, there are other methods of foam prevention, like in situ liquid–liquid extraction, recently presented by Demling et al. (2020). In this approach, the biosurfactant is extracted from the aqueous fermentation broth via a water-insoluble organic solvent. Hence, the biosurfactant can no longer adsorb to gas bubbles, and foam formation is prevented. Another approach combines strain and process engineering: Bator et al. (2020) adapted *P. putida* KT2440 to use ethanol as a carbon source, simultaneously acting as a defoaming agent. However, the mentioned alternative approaches have not been transferred to the biotechnological industry so far. A third approach that allows foam-free aeration without modification of the fermentation system is based on a submerged membrane module. An early example of in situ membrane aeration is the "Lehmann-Reaktor" (Vorlop & Lehmann, 1988) and its later application by Heidemann et al. (1994). This shake flask features in situ membrane aeration for the cultivation of cell cultures and a magnetic stirrer rotating the membrane. The maximum oxygen transfer rate (OTR_{max}) achieved here is 0.9 mmol L^{-1} h^{-1}. A more recent approach with alternating membranes is the "dynamic membrane aeration" presented by Frahm et al. (2007). However, oxygen transfer in these systems was designed for mammalian cell cultivation (Brod et al., 2009), and thus the reported membranes and module designs are insufficient for supplying the high oxygen demands of more than 40 mmol L^{-1} h^{-1} to the microbial rhamnolipid production process.

Recently Bongartz et al. (2021) presented an in situ membrane aeration with an OTR_{max} of 55 mmol L^{-1} h^{-1} for producing rhamnolipids with *P. putida*. The mixing and oxygen entry performance was attained by integrating computational fluid dynamics (CFD) simulations. Using these CFD-optimized membrane aeration modules, foaming could be effectively avoided while producing rhamnolipids (Bongartz et al., 2021).

In this work, we demonstrate that an even higher gas transfer is possible by using the synergistic effects of a stirred membrane module. We rotate the membrane module in the medium and thereby optimize the oxygen transfer at the membrane while using the membrane module to mix the fermentation broth. The membrane-module stirrer (MemStir) is developed in a digital-twin-assisted design process presented in Figure 1. It is initiated by integrating a virtual MemStir draft into the digital twin of a bioreactor. Subsequent interactive CFD-based optimization yields the final design of the MemStir, ready for implementation. This strategy offers a novel approach to predict local oxygen concentrations easily, and shear stresses in the bioreactor before building the actual device. In this work, we further show the architecture and the equipment of the stirrer with gas permeable membrane-mesh blades and provide proof of the feasibility of the MemStir in bench-top bioreactor cultivation of *P. putida* for the foam-free production of rhamnolipids as a pilot process. The applicability of the presented MemStir is shown by cultivation of two different strains of *P. putida* KT2440 in batch and fed-batch mode, which are compared to a regular bubble-aerated process with antifoam addition. The performance of the module regarding gas transfer is examined in several subsequent cultivations, and membrane fouling is characterized via electron microscopy.

2 | MATERIAL AND METHODS

2.1 | Chemicals

In this work, chemicals from Carl Roth GmbH & Co. KG, Merck KGaA, and Sigma Aldrich Chemie GmbH were used. The design and material selection were performed considering the special demands of bioprocesses such as sterilization, biocompatibility, and prevention of dead zones for anti-fouling properties. Further information about the MemStir material and assembly is given in Supporting Information Sections 1.1 and 1.2. The maximum outer diameter of 92 mm was limited by internal installations of the used bioreactor (e.g., two probes with diameters of 10–12 mm), into which the MemStir was integrated (BioFlo 120, Eppendorf, with an inner diameter of 124 mm and a total vessel volume of 3.3 L). The MemStir had a height of 130 mm.

2.2 | Construction of the stirrer module and stirrer setup

The design and material selection were performed considering the special demands of bioprocesses such as sterilization, biocompatibility, and prevention of dead zones for anti-fouling properties. Further information about the MemStir material and assembly are given in SI Sections 1.1 and 1.2. The maximum outer diameter of 92 mm was limited by internal installations of the used bioreactor (e.g., two probes with diameters of 10 to 12 mm), into which the MemStir was integrated (BioFlo 120, Eppendorf, Germany, with an inner diameter of 124 mm and a total vessel volume of 3.0 L). The MemStir had a height of 130 mm.

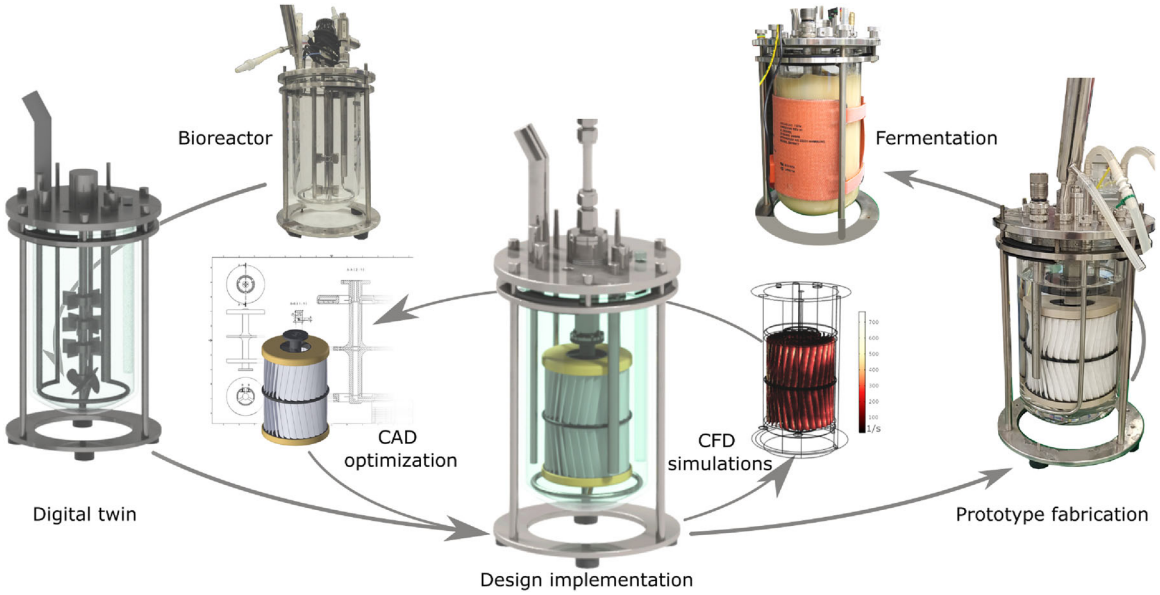

FIGURE 1 Display of the holistic fabrication process: *digitization* of the bioreactor, *implementation* of the virtual MemStir-draft, *CFD simulation* of the drafted installation in regard to mixing-, shear-, and local oxygen conditions, modification of the MemStir-draft and *optimization* towards actual fabrication, *prototype fabrication* and installation in the bioreactor and *characterization* of the MemStir mixing and gas exchange performance in abiotic and fermentative studies.

2.3 | CFD simulations for the evaluation of mechanical stress and mass transfer

Initially, for the simulative investigations of the MemStir, a construction design from purely theoretical considerations was used. Fluid dynamics and mass transport in the MemStir reactor were modeled in COMSOL Multiphysics 5.4 (COMSOL Multiphysics GmbH) to elucidate mechanical stresses and mass transfer limitations in the system. Import of the Inventor Professional 2021 (Autodesk) CAD files in COMSOL, and the required simplification of design elements is described in Supporting Information Section 2.1 in detail. The liquid velocity v in a 3.3-L (total vessel volume, 2 L working volume) MemStir reactor varied from 50 to 500 min^{-1} within this study. In addition, the average $\bar{\gamma}$ and maximum shear rate γ_{max} were determined to investigate the mechanical stress on the organisms. For comparison of the simulated oxygen input to experimental data of previous works (Bongartz et al., 2021), a rotation velocity of 300 min^{-1} was chosen. Here, the average oxygen ($\bar{c}_{O2}$) and the minimum oxygen concentration ($c_{O2,min}$) were examined to assess the oxygen distribution in the reactor.

The assumed oxygen uptake rate (OUR) of 12.8 mmol L^{-1} h^{-1} is a compromise between the actual demand of a *P. putida* KT2440 cultivation (approx. 40 mmol L^{-1} h^{-1} [Demling et al., 2021]), and the presentation of this approach as a universal prediction tool for various bioprocesses: For example, *Corynebacterium glutamicum* is widely used for the production of amino acids and requires an OTR of 15 mmol L^{-1} h^{-1} at a maximal biomass concentration of 9 g L^{-1} (Käß et al., 2014). Schlembach et al. (2020) presented a microbial process for itaconic acid production with *Trichoderma reesei* and *Ustilago maydis*, which demands an OTR of approximately 12 mmol L^{-1} h^{-1}. The here selected OUR derived from a former feasibility study to support the cocultivation approach from Schlembach et al. (2020). The OUR of common cell cultures, such as Chinese hamster ovary (CHO) cells, which are often used to produce therapeutic proteins, is 0.2 mmol L^{-1} h^{-1} at a maximum cell concentration of 8×10^5 cells mL^{-1} (Ducommun et al., 2000).

2.4 | Bacterial strains and media

The bacterial strains *P. putida* KT2440 SK4 (wild type with *att* Tn7:P_{ffg}-*rhlAB*) and the deletion strain *P. putida* KT2440 Δflag SK4 (ΔPP_4328-PP_4344 and ΔPP_4351-PP_4397 with *att* Tn7:P_{ffg}-*rhlAB*) were used for heterologous mono-rhamnolipid production (Blesken, Strümpfler, et al., 2020; Tiso et al., 2020). The strains were recovered in lysogeny broth (LB) (10 g L^{-1} peptone, 5 g L^{-1} yeast extract, and 10 g L^{-1} NaCl). If solid medium was needed, 2% (w/v) agar and 30 µg mL^{-1} gentamycin were added. Pre-cultures for bioreactor cultivations were performed using 10 g L^{-1} glucose and minimal salt medium (MSM) with a final composition (per L) of 11.64 g K_2HPO_4, 4.89 g NaH_2PO_4, 2 g $(NH_4)_2SO_4$, 10 mg EDTA, 100 mg $MgCl_2$ 6 H_2O, 2 mg $ZnSO_4$ 7 H_2O, 1 mg $CaCl_2$ 2 H_2O, 5 mg $FeSO_4$ 7 H_2O, 0.5 mg Na_2MoO_4 2 H_2O, 0.2 mg $CuSO_4$ 5 H_2O, 0.4 mg $CoCl_2$ 6 H_2O, and 1 mg $MnCl_2$ 2 H_2O (modified from Hartmans et al. (1989)). For bioreactor cultivation, the K_2HPO_4/NaH_2PO_4 concentration was reduced threefold. For feeding, a highly concentrated and adjusted MSM was used with a final composition (per L) of 200 g glucose, 7.76 g K_2HPO_4, 3.26 g NaH_2PO_4, 40 g $(NH_4)_2SO_4$, 0.33 g $MgCl_2$ 6 H_2O, 33 mg EDTA, 6.6 mg $ZnSO_4$ 7 H_2O, 3.3 mg $CaCl_2$ 2 H_2O, 16.5 mg $FeSO_4$ 7 H_2O, 0.66 mg Na_2MoO_4 2 H_2O, 0.66 mg $CuSO_4$ 5 H_2O, 1.32 mg $CoCl_2$ 6 H_2O, 3.3 mg $MnCl_2$ 2 H_2O (Demling et al., 2020).

2.5 | Pre-culture preparation

For pre-cultures, *P. putida* KT2440 strains were struck out of a cryoculture on an LB agar plate and incubated for 18 h at 30°C. For liquid cultures, the strains were first recovered in 10 mL LB medium at 30°C at 200 min^{-1} (50 mm throw) with a filling volume of 10%. With the LB culture, a 50 mL MSM pre-culture with 10 g L^{-1} glucose was inoculated to a final optical density (OD_{600}) of 0.1 and cultivated at 30°C at 300 min^{-1} (50 mm throw) with a filling volume of 10%. Cells were harvested in the mid-exponential phase (based on previous experiments at an OD_{600} of 4) to inoculate the bioreactors.

2.6 | Benchmark fermentation with submerged bubble aeration

Batch fermentation for rhamnolipid production with submerged bubble aeration was conducted in a BioFlo 120 glass bioreactor (Eppendorf) with a working volume of 1.2 L and a nominal volume of 3.3 L. The process was regulated by a control unit (BioFlo 120) and DASware control software (v 5.3.1) (Eppendorf) (see also Figure 2). The bioreactor was equipped with a pH probe (EasyFerm Plus PHI 225), dissolved oxygen (DO) probe (VisiFerm DO ECS 225), and a Pt100 temperature sensor. The agitator shaft was equipped with two Rushton turbines (Ø 5.3 cm). As a countermeasure against foam formation due to rhamnolipid production, antifoaming agent 204 (Sigma-Aldrich) was constantly pumped into the reactor (0.5–3.0 mL h^{-1}). The batch cultivations were conducted in MSM with 10 g L^{-1} of glucose as the sole carbon source. The pH value of 7 was kept constant by automatic addition of 4 M KOH/H_2SO_4 via peristaltic pumps. The DO was maintained above 30% by automatically increasing the stirring rate from 300 to 1200 min^{-1}. The gas flow through the ring sparger was constant at 0.12 L min^{-1}. The temperature was set to 30°C. The reactor was inoculated with cells from an MSM pre-culture to an OD_{600} of 0.2.

2.7 | Membrane-module stirrer for bubble-free aeration: Fermentation conditions

Batch and fed-batch cultivations for rhamnolipid production in a MemStir bioreactor for bubble-free aeration were conducted with the same bioreactor equipment and standard parameters (T, pH, media, and

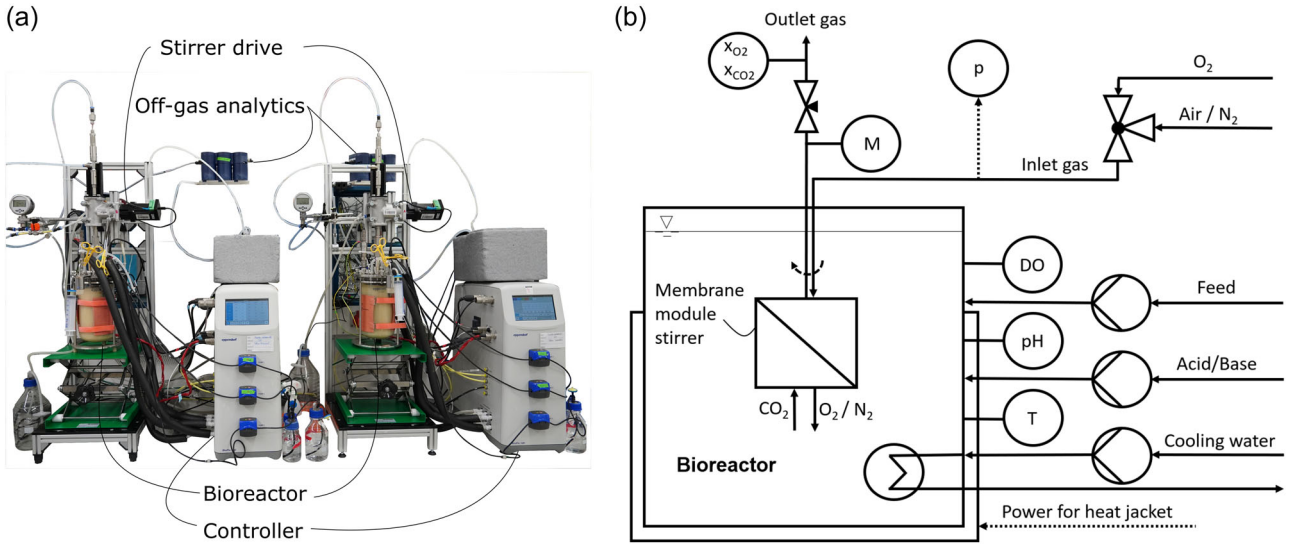

FIGURE 2 (a) Picture of the cultivation setup for parallel fermentation. Fermentations were conducted in a 3.3-L BioFlo 120 glass bioreactor (Eppendorf). The process was regulated by a control unit (BioFlo 120). Off-gas was analyzed with a BlueVary gas analyzer (BlueSens). (b) Simplified process scheme of the bioreactor setup including the stirrer drive (M), the pressure gauge (p), oxygen probe (DO), pH probe (pH), temperature probe (T), and the off-gas analytic (X_{O2} and X_{CO2}).

inoculation procedure) as described in Section 2.5. The working volume was increased to 2.0 L. A MemStir was used as the mixing and aeration unit for bubble-free aeration. The stirrer drive for MemStir agitation was obtained from Nanotec Electronic (PD4-C5918L4204-E-01) with an H2 i = 1:1 bevel gear from Mädler and a claw coupling and motor flange (both from igus).

For sterilization, the reactor was autoclaved without liquid at 121°C and 2 bar pressure without the MemStir. The MemStir was sterilized separately with 70% ethanol. After the autoclaving process, the MemStir was mounted into the reactor on a clean bench. Afterward, the sensors were added after disinfection with 70% ethanol. If the membrane module was used several times, it was sterilized with 70% ethanol and then cleaned with water. The MemStir was operated in cross-flow mode. The DO was maintained above 30% (1) by manually increasing the stirring rate from 100 to 300 min^{-1}, (2) by manually increasing the transmembrane pressure (TMP) from 0 to 0.3 bar, and (3) by automatically increasing the amount of oxygen in the supply air (X_{O2} = 21% to 100%). The gas flow through the MemStir was constant at 1 L min^{-1}. The carbon dioxide and the oxygen concentrations at the outlet of the MemStir were measured by BlueVary gas analyzer, and data was recorded with BlueVis (both BlueSens). In addition to batch cultivations, fed-batch cultivations were performed using a DO-based C-limited feeding strategy. The feeding pump was activated when the DO signal increased, indicating a carbon source depletion. At a DO of 70%, the pump rate was set to 48 mL h^{-1} resulting in an addition of feed solution and a decrease in the DO. At a DO of 60%, feeding was stopped until the carbon source was again depleted, and 70% was reached. A total of 250 mL concentrated feed solution (Section 2.3) was added throughout the fermentation. The initial volume was set to 2 L MSM. The setpoint of X_{O2} was manually increased to avoid oxygen limitations when the DO decreased below 10%. All other parameters were set as described for batch cultivations.

2.8 | Analysis of bacterial growth

Bacterial growth was determined by measuring the OD_{600} at 600 nm with the Ultrospec 10-cell density meter (BioChrom). A correlation between OD_{600} and cell dry weight (CDW) was established. A CDW of 313 mg L^{-1} corresponds to an OD_{600} of 1.0 (6-point calibration with n = 3).

2.9 | Analysis of ammonium

Ammonium concentrations in the supernatant were analyzed via colorimetric determination using salicylate. The assay was modified according to Willis et al. (1996). The reagent solution consisted of (per L) 32 g Na-salicylate, 40 g Na_3PO_4 12 H_2O, and 0.5 g Na-nitroprusside. Ammonium sulfate standards between 5 and 200 mg L^{-1} were prepared for calibration. For the measurement, each well of a 96-well plate (Greiner CELLSTAR, MERCK KGaA) was first filled with 10 µL of standard solution or diluted sample, then 200 µL of reagent solution and at last 50 µL 5% NaClO solution were added. After an incubation time of > 12 min at room temperature, the samples were analyzed in a Synergy MX plate reader (BioTek Instruments) at a wavelength of 685 nm.

2.10 | Analysis of glucose, gluconate, and 2-ketogluconate

To quantify the concentration of glucose, gluconate, and 2-ketogluconate (2-KG), samples from the reactor were analyzed by high-performance liquid chromatography (HPLC). The detailed HPLC method was presented by Tiso et al. (2020).

2.11 | Analysis of rhamnolipids

Reversed-phase chromatography coupled to Corona Charged Aerosol Detection was performed to quantify mono-rhamnolipid, and 3-(3-hydroxyalkanoyloxy)alkanoate (HAA) concentrations based on a previously developed method (Behrens et al., 2016; Tiso et al., 2020). However, the gradient of the method was slightly modified. Acetonitrile (A) and 0.2% (v/v) formic acid in ultra-pure water (B) was used as running buffers. The method started with a 70% buffer A:30% buffer B ratio, and a linear gradient was applied to reach a ratio of 80%:20% in 8 min. The acetonitrile ratio increased linearly from 80% to 100% between 9 min and 13 min and decreased linearly to 70% between 16 min and 17.5 min. The measurement was stopped after 20 min. The term "rhamnolipid" hereafter relates to the resulting natural mixture containing mono-rhamnolipids and a small fraction of the aglycone HAAs.

2.12 | Extraction of antifoaming agent

The antifoaming agent was extracted since even low concentrations in the fermentation broth negatively affect the measurement of OD_{600}, CDW, and rhamnolipid concentration (Demling et al., 2020). For the extraction, 400 µL n-hexane was added to 1 mL sample. The sample was mixed, and after centrifuging at 13,000 *g* for 2 min, two phases formed. The upper phase was discarded. This procedure was repeated until the lower phase was clear.

2.13 | Sample preparation for FESEM

Samples were prepared by immersing the modules gently in 70% (v/v) ethanol for 30 min. Afterward, the modules were dried in an oven at 30°C for 8 h. Pieces of the membrane meshes were cut out, fixated on a sample carrier, and sputtered. Samples were sputtered with a Quorum Q300TTPlus (Judges Scientific plc) with Au/Pd (80:20) for 100 s. Finally, samples on the carrier were loaded in the Schottky Field Emission Scanning Electron Microscope ((FESEM) SU5000, Hitachi).

3 | RESULTS AND DISCUSSION

Recent membrane-aeration systems did not prevail in biotechnology outside of their applied niche. This is mostly due to their inadequate support for oxygen-demanding processes. To engineer a membrane module, which fulfills demands in gas transfer and medium mixing, the geometry of the bioreactor vessel and installations has to be considered. Therefore, a digital twin of the utilized bioreactor was designed (see Figure 1). In this digital twin, the MemStir was fitted. The respective design of the MemStir was iteratively developed by CFD simulations and computer-aided design (CAD) optimizations. Here, we present the final design and construction of the MemStir. At first, we show the CFD characterization of this geometry as a result of the optimization, and secondly, the final design. Finally, *P. putida* cultivations demonstrate the performance of the MemStir, compared with a bubble-sparged benchmark.

3.1 | The simulative optimized membrane-module stirrer design

Before prototyping the MemStir, simulations were performed to validate the function of the stirrer module for mixing and oxygen transfer. To estimate mass transfer, the flow conditions, and possible shear stress on the organisms, multiphysics simulations were performed according to Section 2.2. To characterize the applicability of the MemStir in different bioprocesses, flow conditions, and shear rates at different locations in the bioreactor were examined. The three-dimensional (3D) simulated model was sliced in a two-dimensional (2D) to present the findings. Figure 3a shows a 3D CAD sketch for the orientation of the examined locations.

The velocities depicted in a 2D plot of a horizontal cross-section (Figure 3b) indicate gradients in the flow velocity by a stirring rate of 500 min^{-1}. The outer regions expose small areas of velocities below 0.25 m s^{-1} (in black) directly behind the installations. The velocity is highest at the outer end of the membrane blades with approximately 1.4 m s^{-1}. The horizontal cross-section at various stirrer rotation speeds in Figure 3c reveals higher velocities in the volume between the MemStir blades. Depicted flow direction arrows present the development of vortices between the MemStir and the bioreactors wall. Four axis-symmetric vortices are apparent above a stirring rate of 200 min^{-1}. Vortices on the left side of the axis are highlighted by gray arrows in the image of the stirring rate of 500 min^{-1} in Figure 3c. Vortices evolve as the stirring rate increases. Although this observation already gives a visual indication of mixing in the bioreactor, the overall velocity was calculated via simulation. The average velocity $\bar{v}$ is shown in Figure 4a regarding the stirring speed.

The minimum oxygen concentration $c_{O2,min}$ varies between 0.044 mmol L^{-1} (200 min^{-1}) and 0.052 mmol L^{-1} (500 min^{-1}). The average oxygen concentration $\bar{c}_{O2}$ is 0.051 mmol L^{-1} for 200 min^{-1} and 0.054 mmol L^{-1} for 500 min^{-1} by simulated aeration with air at 30°C (see Supporting Information Section 2.4).

To virtually compare flow conditions of the dynamic MemStir to the static module of Bongartz et al. (2021), the circumferential speeds of the stirrers have to be equalized. Therefore, the MemStir is set here to a stirring rate of 170 min^{-1}, while the stirrer in the middle of the static membrane module was set to 300 min^{-1} (maximum stirrer rate tested). By this, the circumferential speeds of the rotating elements are both adjusted to 0.84 m s^{-1}. The average speed of the liquid $\bar{v}$ results in 0.2 m s^{-1} for the static module and 0.3 m s^{-1} for the rotating MemStir. Mechanical efficiency of the MemStir for mixing is therefore demonstrated because Bongartz et al. (2021) already showed effective mixing in the bioreactor at lower $\bar{v}$. To assess the shear stress on the organisms, shear rates on the membrane blades were calculated. Figure 3d visualizes the results of a simulation with a stirring rate of 200 min^{-1}. A detailed view of a single membrane blade

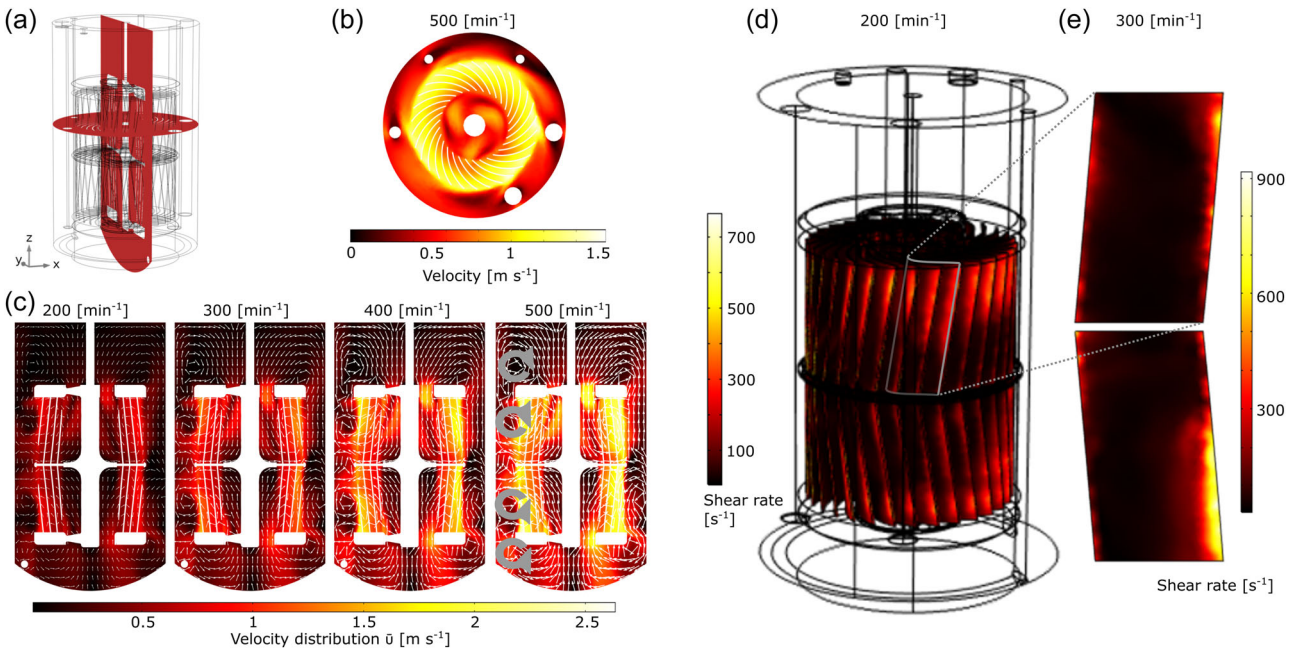

FIGURE 3 CFD characterization of the MemStir design. (a) Display of the presented cross-section in (b) and (c). (b) Horizontal cross-section of a simulation for the study of the local velocities at a stirring rate of 500 min^{-1}. (c) Comparative study of several stirring rates from 200 to 500 min^{-1}, the white arrows indicate the flow direction. (d) 3D model of the MemStir with indicated shear rates on the membrane-mesh blades. (e) Shear rate distribution on a single membrane-mesh blade at a stirring rate of 300 min^{-1}. CFD, computational fluid dynamics.

is given in Figure 3e, using a stirring rate of 300 min^{-1}. The shear rate reaches the highest values in the outer regions of the single blade. By beveling the membrane blades, the maximum shear rate was reduced from 1628 to 1263 s^{-1}. The average shear rate $\bar{\gamma}$ of all membrane surfaces was linear in the examined stirrer rate range between 50 and 500 min^{-1} (see Figure 4a). According to Menniti et al. (2009), shear rates below 1800 s^{-1} pose no harm to shear-sensitive animal cells.

Bacteria and most yeasts are very robust against shear forces. As shear forces are induced only by the stirrer in the MemStir reactor (no bubble rupture), stirrer tip speeds can be used as an indicator for the intensity of shear forces. For comparison, stirrer tip speeds are given in the literature. With a radius of approximately 90 mm and 500 min^{-1}, the circumferential speed of the outer membrane is 2.36 m s^{-1}. This speed is at the lower end of stirrer tip speeds in regular industrial applications. For example, for 100 L *Escherichia coli* cultivations, stirrer tip speeds between 2 and 5 m s^{-1} are used (Schirmer et al., 2017). Cultivation of hyphae-building *Penicillium chrysogenum* for penicillin production in agitated vessels of 0.005–1 m^3 showed no harm at this impeller tip speeds in the main cultivation phase (Makagiansar et al., 1993).

The oxygen supply and mass transport in the bioreactor were studied by spatially resolving the oxygen concentration. Here, oxygen supply is realized by setting a fixed oxygen concentration at the membrane surface, while oxygen consumption occurs in the bulk medium. Detailed information about the simulation method is given in Section 2.2. Figure 5a depicts the vertical and horizontal cross-section of the simulation results. The lowest molar oxygen concentration is found in the center of the stirrer, as indicated by Figure 5b. This corresponds to the flow dynamics in Figure 3c. Oxygen-poor medium is transported from the inlets in the (top and bottom) caps to the membrane, which is enriched with oxygen and pushed into the outer region of the stirrer and in the outer compartment of the vessel. Figure 5c displays the relationship between stirring rate and (local) oxygen concentration. The color scale resolves a comparable small concentration scale to ease the presentation of the marginal differences at different stirring rates. The minimum oxygen concentration $c_{O2,min}$ varies between 0.044 mmol L^{-1} and 0.052 mmol L^{-1}. The average oxygen concentration $\bar{c}_{O2}$ ranges from 0.051 mmol L^{-1} for 200 min^{-1} to 0.054 mmol L^{-1} (see Figure 4a). To classify these findings, the virtual oxygen supply (OUR = 12.8 mmol L^{-1} h^{-1}) from the CFD simulation is compared to the demands of typically used organisms in biotechnology: The results indicate that CHO cells, which are common in animal cell cultivation (with an OTR of approx. 0.2 mmol L^{-1} h^{-1} per 8×10^5 cells mL^{-1}) (Ducommun et al., 2000) would be sufficiently supplied with oxygen. Plant cell cultivations with their comparably lower oxygen demand per gram CDW (0.5 $mmol_{O2}$ g_{CDW}^{-1} h^{-1}, Seidel et al., 2021) could be supported up to approximately 38.5 g_{CDW} L^{-1}. For evaluation of the virtual support of microbial processes, specific OUR values were taken from *E. coli* (2.95 $mmol_{O2}$ g_{CDW}^{-1} h^{-1}) and *Saccharomyces cerevisiae* (1.34 $mmol_{O2}$ g_{CDW}^{-1} h^{-1}) from Seidel et al. (2021). In the simulated cultivation volume of 2 L, the MemStir could support a process with up to 6.5 g_{CDW} L^{-1} *E. coli* or approximately 14.5 g_{CDW} L^{-1} *S. cerevisiae*. Even though the oxygen transfer rate will not support high cell-density bacteria or fungi cultivations, it is suitable for many bioprocesses, like the production of rhamnolipids with *P. putida*, possibly for the cost of a prolonged cultivation time (compare Demling et al., 2021 with a specific oxygen demand of around 12.5 $mmol_{O2}$ g_{CDW}^{-1} h^{-1}).

After simulative optimization and characterization, the real-life validation of the MemStir was followed up.

Derived from CFD simulations and former designs, the hollow fiber membranes are inserted in the form of blades in curved slots. The function is comparable to a centrifugal pump, and the membrane is rotated in the medium. By the permanent agitation of the membrane, the concentration polarization of the gasses on the surface of the membrane is decreased. Due to the mesh-like structure of the membrane elements, these elements function as stirrer blades and mix the medium while exchanging oxygen and carbon dioxide by the intrinsic permeability of the membrane's material (Allen et al., 1977) (see Figure S2). By the blade-shaped arrangement of the membrane elements, the liquid is transported in a radial direction. The design and operating principle in a cross-flow mode of the MemStir are demonstrated in longitudinal, cross-section, and partial view in Figure 6a–e. Geometric dimensions are given in Supporting Information Chapter 1.2. A total of 30 membrane slots are circularly arranged around the drive axis of the module, equally arranged by 12° (Figure 6e). 55 hollow fiber membranes can be integrated into each of the existing slots, resulting in a total membrane area of approximately 2090 cm^2. The number and angle of the membrane elements are a compromise between the largest membrane surface, media transport, and fabrication options. By simulation, angles and number of membrane elements were compared (Data not shown). Figure 6a–c demonstrates the gas exchange concept of the MemStir. Cavities in the lids and the shaft supply discharge the gas in the MemStir (compare Figure 6c). Because of the internal gas circulation, the MemStir can be flown through permanently (in cross-flow mode) to increase the gas exchange by keeping a constantly high trans-membrane concentration gradient of oxygen and carbon dioxide. The design of this MemStir is enhanced with a disc on the upper gas connection. This disc prevents eddy formation during operation (not shown).

To characterize the oxygen transfer of the developed MemStir, the OTR_{max} was determined. The OTR was calculated by the maximum slope of the measured dissolved oxygen concentration between 0% and 100% oxygen (with 7.5 mg L^{-1} as 100%). For MemStir directly after fabrication, an OTR_{max} of 175 mmol L^{-1} h^{-1} was achieved (Figure 4b). After one fermentation, the OTR_{max} was 120 mmol L^{-1} h^{-1} and after a subsequent fermentation, OTR_{max} was 95 mmol L^{-1} h^{-1}. To investigate the reason for the performance loss, membrane samples were analyzed by electron microscopy. Figure 7a shows a plasma-activated PMP hollow fiber as reference. The images of Figure 7b show debris residues on a hollow fiber of a MemStir after one fermentation, probably originating from *P. putida*. These residues appear to be spread more homogeneously on the membrane of a module used for two fermentations (Figure 7c) and demonstrate the stability of the process as no significant increase in biofouling is visible. To demonstrate the feasibility of the MemStir and to compare it with a regular bubble-sparged process, several cultivations were conducted with *P. putida* KT2440 strains producing rhamnolipids.

(a)

Stirring speed [min^{-1}]	$\bar{v}$ [m s^{-1}]	$\bar{\gamma}$ [s^{-1}]	$c_{O_2,min}$ [mmol L^{-1}]	$\bar{c}_{O_2}$ [mmol L^{-1}]
50	-	8.20	-	-
200	0.31	43.38	0.044	0.051
300	0.47	64.32	0.048	0.052
400	0.63	85.02	0.049	0.053
500	0.78	107.06	0.052	0.054

(b)

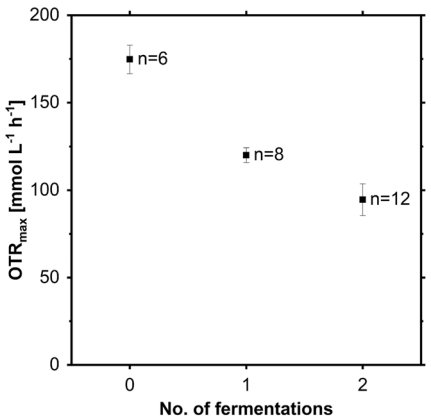

FIGURE 4 Characterization of the MemStir Module virtual via CFD simulations (a) and in real-life OTR measurements (b). (a) Display of the average velocity $\bar{v}$, average shear rate $\bar{\gamma}$, the minimum oxygen concentration $c_{O2,\ min}$ and the average oxygen concentration $\bar{c}_{O2}$ at different stirring rates in the simulated bioreactor with the MemStir. (b) Maximum oxygen transfer capacity (OTR_{max}) of MemStirs after their application in increasing numbers of fermentations, with *n* = number of measurements. CFD, computational fluid dynamics.

3.2 | Benchmark fermentation for rhamnolipid production

First, benchmark cultivation with submerged bubble aeration for rhamnolipid production was performed. To control the foaming caused by the bubble aeration, undiluted antifoaming agent (Antifoam 204, Sigma-Aldrich) was continuously dosed into the reactor. The fermentation was conducted in biological duplicates with *P. putida* KT2440 Δflag SK4 for 10 h. This strain was selected since it has previously achieved one of the highest rhamnolipid titers of 1.5 g L^{-1} in recombinant rhamnolipid production (Tiso et al., 2020). By knocking out the genes responsible for the synthesis of the flagellar machinery required for motility, the strain saves resources that can be fed into rhamnolipid production (Martínez-García et al., 2014). The energy-saving strain is also of interest for bioprocesses with foam formation since knocking out the flagellum genes alters the cell surface by becoming less hydrophobic. Less hydrophobic cells are more likely to remain in the culture broth and not attach to the air bubbles in the foam (Blesken, Bator, et al., 2020; Martínez- García et al., 2014). Figure 8b shows the course of the CDW, glucose, ammonium sulfate, and rhamnolipid concentrations during the fermentation. A maximum CDW of 3.12 g L^{-1} with a μ_{max} of 0.46 h^{-1} was achieved. After 7 h, the glucose was depleted, and about 6.0 g L^{-1} 2-ketogluconate (2-KG) was accumulated in the

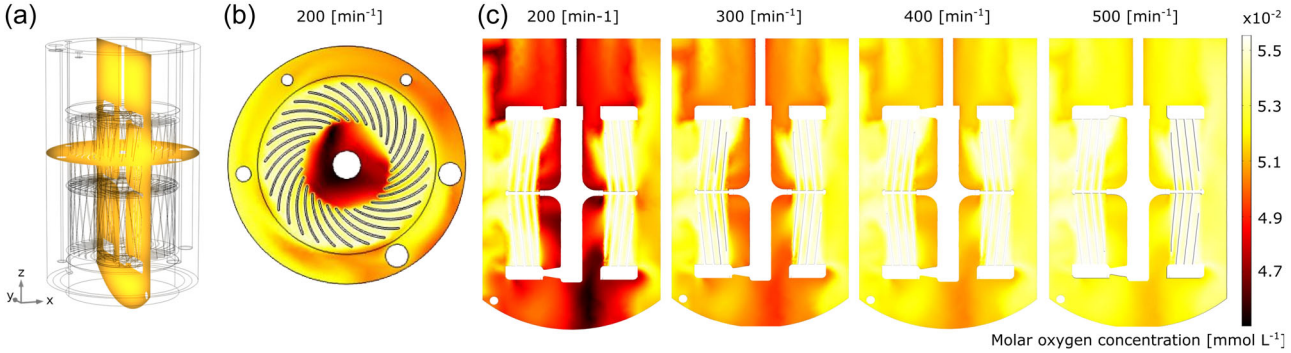

FIGURE 5 Investigation of the oxygen supply by the MemStir via CFD. (a) Display of the presented cross-sections in (b) and (c). (b) Horizontal cross-section of a simulation of the local oxygen concentration at a stirring rate of 200 min^{-1}. (c) Comparative study of several stirring rates from 200 to 500 min^{-1}. CFD, computational fluid dynamics.

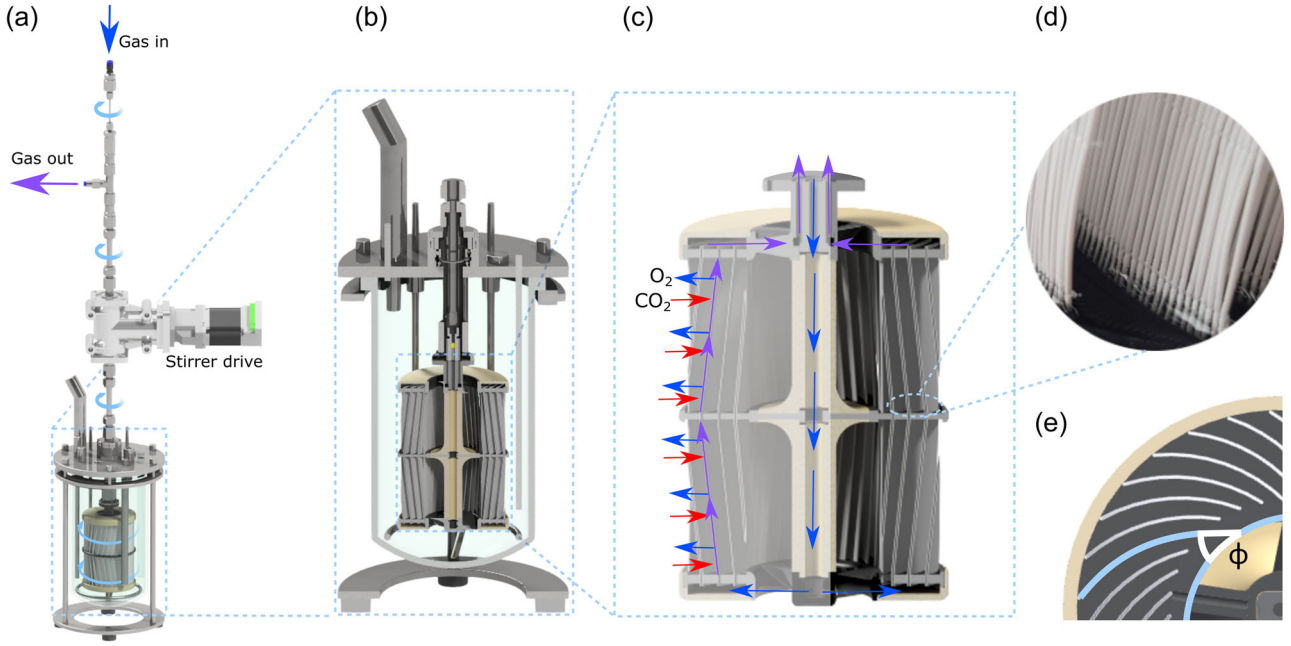

FIGURE 6 Scheme of the membrane-module stirrer (MemStir) unit. (a) MemStir is installed in the bioreactor and connected to the gas piping and the stirrer drive. (b) Vertical cross-section of the bioreactor with the MemStir. Regular probe positioning is considered. (c) Focused view on the MemStir with the highlighted gas flow through the MemStir. The inlet flow of air/oxygen (blue arrows), the intake of carbon dioxide (red arrows), and the stream of the outgoing gas mixture (purple arrows) are visualized. (d) Close-up photo of the membrane-mesh slots including the PMP membrane. (e) Schematic top view of the membrane mounting, marking the angle of incident ϕ (=43°) for membrane-mesh blades integration.

culture broth (Figure S1A). The average volumetric glucose uptake rate was 1.51 g_{Glc} L^{-1} h^{-1}. Afterward, the strain showed a lower growth rate on gluconate and 2-KG. Both are produced in the periplasm as intermediates of the glucose metabolism in *P. putida* (Blank et al., 2008). At the end of the fermentation, a rhamnolipid titer of 0.33 g L^{-1} was achieved. Figure 8c shows the DO and the stirring rate. By automatically adjusting the stirring rate, the DO was maintained at or above 30%. The stirring rate increased until 6.5 h to 750 min^{-1} and decreased rapidly to the initial conditions thereafter. This drop correlates to the glucose data, as the glucose was depleted at this point. Subsequent growth on gluconate and 2-KG caused the agitation to rise to approximately 500 min^{-1}. The fermentation was stopped after 10 h, although about 2 g L^{-1} of 2-KG was still present (Figure S1A). The samples could not be further processed due to the formation of large interphases during n-hexane extraction, caused by increasing rhamnolipid and CDW concentrations and the addition of 27.9 mL of antifoaming agent (23 g L^{-1}). The large interphase also likely caused a significant underestimation of rhamnolipids (Demling et al., 2020). However, a product-to-substrate yield ($Y_{P/S}$) of 0.04 g_{RL} g_{Glc}^{-1} was obtained with this bioreactor setup. Furthermore, a space-time yield (STY) of 36 mg_{RL} L^{-1} h^{-1} was reached. Compared with the fermentation with continuous foam recirculation and

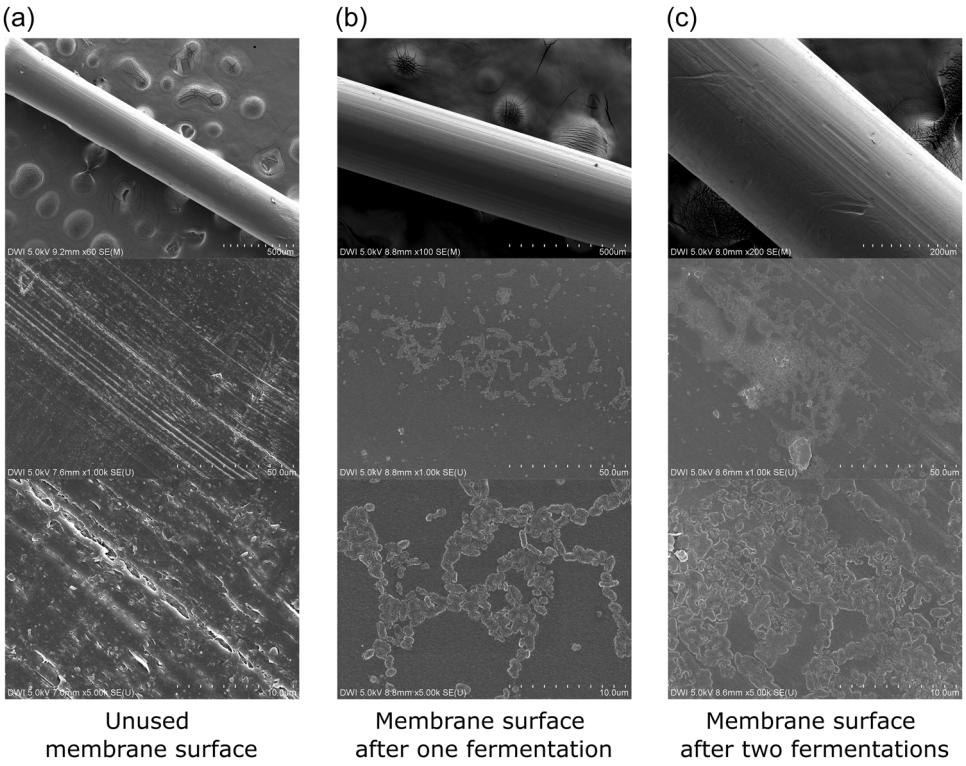

FIGURE 7 FESEM pictures of the utilized PMP Oxyplus hollow-fiber membranes (3 M). (a) Plasma-activated membrane as present in a freshly prepared MemStir. (b) Membrane after one fermentation. (c) After two fermentations with *P. putida* and subsequent ethanol immersion (compare Section 2.12).

10 g L^{-1} glucose with the energy-saving strain (Tiso et al., 2020) the $Y_{P/S}$ here is 0.3-fold lower while the STY is 0.2-fold lower.

The benchmark fermentation shows how complex the process control and the processing of samples with antifoaming agent is. Apart from challenges in analytics, the antifoaming agent will also affect down-stream processing because the separation of rhamnolipids and antifoaming agent is intensely elaborate (Jiang et al., 2020; Junker, 2007; Sha et al., 2012). In addition, the headspace of the bioreactor was filled with foam (Figure 8a), which slowed down the process as part of the whole-cell biocatalysts were dispended in the foam phase and probably exposed to limitations. In addition, most likely, rhamnolipids will accumulate in the foam phase because of their foaming-out effect (Blesken, Bator, et al., 2020).

3.3 | Membrane-module stirrer for foam-free production of rhamnolipids

After the benchmark fermentation with bubble aeration and antifoaming agent addition, the MemStir was tested in batch mode to compare the influence of the two different aeration methods on oxygen supply, rhamnolipid production, and foam formation. While similar in batch fermentation, the performance of the two strains (*P. putida* KT2440 SK4 and *P. putida* KT2440 Δflag SK4) significantly differed in fed-batch fermentation. In contrast to the benchmark fermentation, no antifoaming agent was added, and hence n-hexane extraction could be omitted.

3.3.1 | Rhamnolipid production with *P. putida* KT2440 SK4 in batch mode

The MemStir batch fermentation was conducted in biological duplicates with *P. putida* KT2440 SK4 for 10 h. The MemStir replaced the stirrer and ring sparger as the mixing and aeration unit for bubble-free aeration of the bioreactor (Figure 2). Figure 8e shows the CDW, glucose, ammonium sulfate, and rhamnolipid concentrations. A maximum biomass concentration of 2.57 g L^{-1} with a μ_{max} of 0.59 h^{-1} was achieved. While the biomass concentration is lower than in the benchmark fermentation, the growth rate is 1.3-fold higher. After 9 h, the glucose was depleted, and only small amounts (<0.5 g L^{-1}) of gluconate and 2-KG were accumulated in the culture broth (Figure S1B). The volumetric glucose uptake rate was 1.09 g_{Glc} L^{-1} h^{-1}, which is 0.7-fold lower compared to the benchmark fermentation. At the end of the fermentation, a rhamnolipid titer of 1.17 g L^{-1} was achieved, which is a measured 3.5-fold higher titer than in the benchmark fermentation. Due to the antifoaming agent, the rhamnolipid concentration in the benchmark fermentation is underestimated by the n-hexane extraction and the subsequent

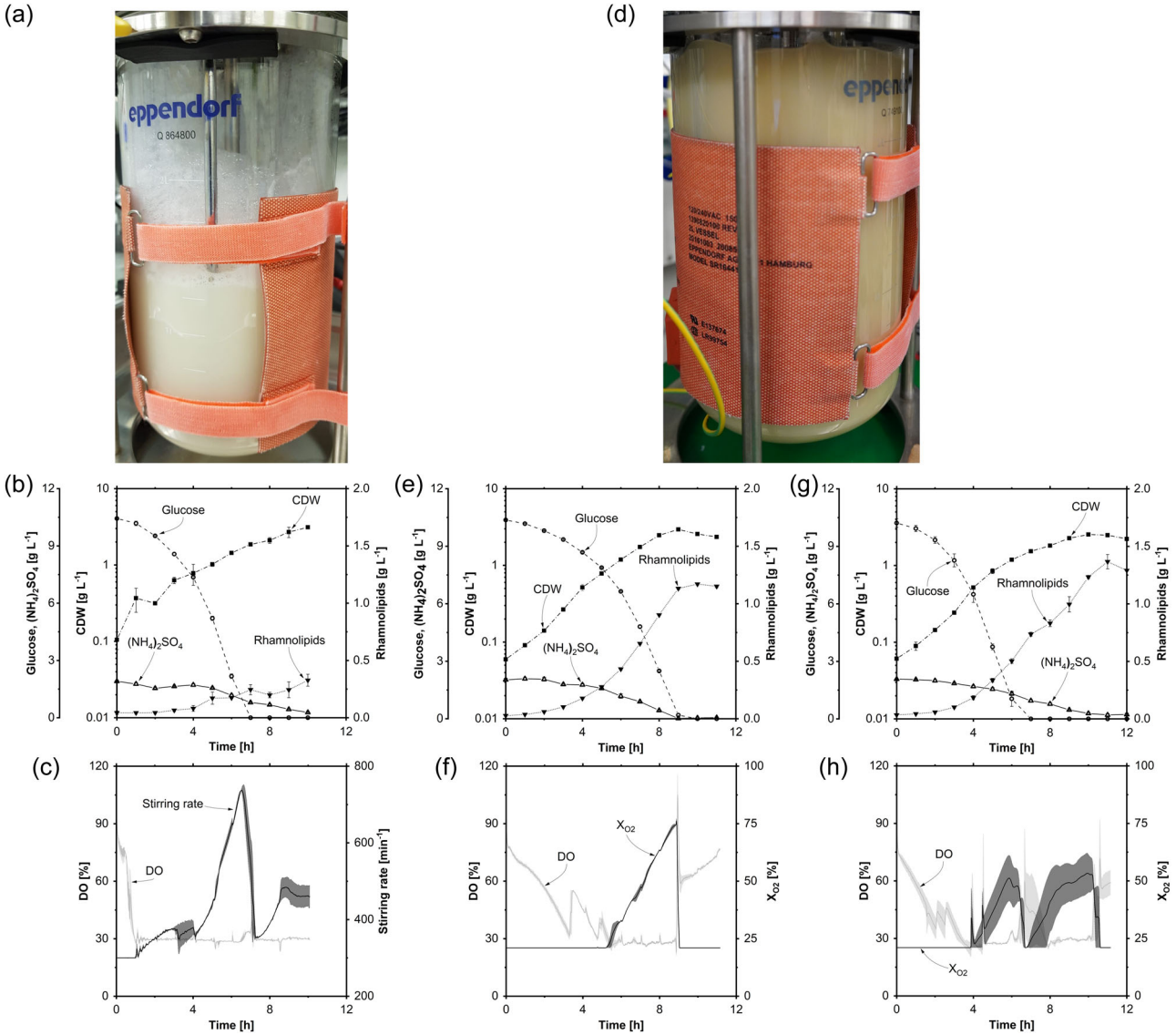

FIGURE 8 Results of three different rhamnolipid production batch fermentations with conventional submerged bubble aeration (a–c) and bubble-free aeration with a membrane-module stirrer (MemStir) (d–h). The batch fermentations were conducted in MSM using 10 g L^{-1} glucose at 30°C at pH 7 and inoculated with an OD_{600} of 0.2. The total reactor volume was 3.3 L. For the benchmark fermentation, the cultivation volume was 1.2 L, the aeration rate was 0.12 L min^{-1}, and the stirring rate was between 300 and 800 min^{-1}. For the cross-flow MemStir fermentations, the cultivation volume was increased to 2.0 L, the aeration rate was 1.0 L min^{-1}, the stirring rate was between 100 and 300 min^{-1}, and the transmembrane pressure (TMP) was between 0 and 300 mbar (Section 2.6). (a) Exemplary picture of the bioreactor with foam formation during the benchmark fermentation with conventional bubble aeration. (b) Trend of CDW, rhamnolipid, glucose, and $(NH_4)_2SO_4$ concentrations in the benchmark fermentation using the KO strain *P. putida* KT2440 Δflag SK4. (c) Corresponding online signals of dissolved oxygen (DO), and stirring rate to graph (b). (d) Exemplary picture of the bioreactor during the MemStir fermentation without foam formation. (e) Concentrations of CDW, rhamnolipid, glucose, and $(NH_4)_2SO_4$ in the MemStir batch fermentation using *P. putida* KT2440 SK4. (f) Corresponding online signals of DO and X_{O2} (oxygen content in the supply air) to graph (e). (g) Trends of CDW, rhamnolipid, glucose, and $(NH_4)_2SO_4$ concentrations in the MemStir batch fermentation using the KO strain *P. putida* KT2440 Δflag SK4. (h) Corresponding online signals of DO and X_{O2} to graph (g). The error bars and error bands show the minimum and maximum values of two individual cultivations.

HPLC analytics. It is essential that the culture volume is 1.7-fold higher in contrast to the benchmark fermentation, as the headspace of the MemStir bioreactor does not have to be kept free for eventual foam formation. Thus, higher product amounts per batch can be achieved. Figure 8f shows the DO and the X_{O2} of the supply gas. The DO was maintained at 30% throughout the cultivation. The DO increase at 3 h corresponds to the manual increase of the stirrer rate from 100 to 300 min^{-1}, and the second DO increase at 4.5 h to the manual rise of the TMP from 0 to 300 mbar. After that, the share of pure oxygen in the inlet gas was automatically increased to keep the

DO at 30%. The DO peak at 9 h correlates with glucose depletion, leading to an abrupt increase in DO and an abrupt decrease in the oxygen content of the inlet gas. The maximum oxygen content of the supply gas was approximately 75%. Neither foam formation nor oxygen limitation were observed over the fermentation time. A $Y_{P/S}$ of 0.11 $g_{RL}\ g_{Glc}^{-1}$ was obtained, 2.8-fold higher than in the benchmark fermentation. Furthermore, a STY of 118 $mg_{RL}\ L^{-1}\ h^{-1}$ until glucose depletion was reached, 3.3-fold higher than in the benchmark fermentation.

3.3.2 | Improving energy efficiency leads to increased productivity

The second MemStir batch fermentation was conducted in biological duplicate with the energy-saving strain *P. putida* KT2440 Δflag SK4 for 11 h. Figure 8g shows the CDW, glucose, ammonium sulfate, and rhamnolipid concentrations. A maximum biomass concentration of 2.49 g L^{-1} with a μ_{max} of 0.61 h^{-1} was achieved, which is comparable with the first MemStir batch fermentation with *P. putida* KT2440 SK4. The glucose was also converted within 7 h as in the benchmark fermentation. The volumetric glucose uptake rate of 1.52 $g_{Glc}\ L^{-1}\ h^{-1}$ is also similar. After 11 h of fermentation, the rhamnolipid titer was 1.37 g L^{-1}, 1.2-fold higher than in the *P. putida* KT2440 SK4 cultivation and 4.2-fold higher than in the benchmark fermentation, although the same strain was used. The latter might have been caused due to the extraction of the samples with n-hexane or a potential negative effect of antifoaming agent addition. The physiological data show that the system with the MemStir is more suitable for producing rhamnolipids than a setup where the addition of antifoaming agent is required. Figure 8h shows the DO and the X_{O2} of the supply air. The DO was maintained at 30% in the same manner as the *P. putida* KT2440 SK4 cultivation. The supplemented oxygen in the supply gas increased from 3.5 to 6.5 h and then dropped abruptly to the initial conditions. This drop is caused by glucose depletion, while the subsequent increment is induced by growth on gluconate and 2-KG. This diauxic growth behavior was also observed during the benchmark fermentation with the energy-saving strain but not in the *P. putida* KT2440 SK4 cultivation. In contrast to the SK4 strain, the energy-saving strain produces significantly more 2-KG and converts glucose to 2-KG first, accumulating it in the culture broth (Figure S1B,C). The accumulation of 2-KG in the deletion strain could be due to an imbalance in the equivalent redox balance. The flagellum stator pumps protons into the cell for its operation, and these are then pumped back out of the cell by the electron transport chain to keep the proton-motive force and keep the pH constant in the cytosol (Martínez- García et al., 2014; Minamino & Imada, 2015). By oxidizing glucose in the periplasm to 2-KG, *P. putida* generates two reduced pyrroloquinoline quinones ($PQQH_2$) (Blank et al., 2010; Nikel et al., 2015). Thus, *P. putida* generates reducing power by the oxidation of glucose to 2-KG. 2-KG is re-released, while $PQQH_2$ is reoxidized by sequential single electron transfer to a type c cytochrome in the electron transport chain to yield ATP (Blank et al., 2010). This could be a reason that the deletion of the flagellum disturbs the redox balance; thus, the strain reacts by diverting carbon. However, this is only a hypothesis and needs to be investigated with further experiments. The maximum oxygen content in the supply gas was at approximately 50%, which is 0.7-fold lower than in the *P. putida* KT2440 SK4 fermentation (compare Figure 8f). The lower oxygen consumption could be related to the knockout, as the energy-saving strain no longer has a flagellum and thus requires less energy (Martínez-García et al., 2014). Furthermore, the energy-saving strain grew exclusively on 2-KG (6.5 g L^{-1}) after 6 h of cultivation (Figure S1C). On 2-KG, the energy-saving strain showed a lower growth rate (μ_{2KG} of 0.20 h^{-1}) than on glucose, therefore, the strain consumed less oxygen per hour, and the process is prolonged. No foam formation and oxygen limitation were observed during the cultivation. A $Y_{P/S}$ of 0.13 $g_{RL}\ g_{Glc}^{-1}$ was obtained, 1.2-fold higher than in the *P. putida* KT2440 SK4 cultivation. Furthermore, a STY of 124 $mg_{RL}\ L^{-1}\ h^{-1}$ until glucose depletion was reached, which is 1.1-fold higher than in the *P. putida* KT2440 SK4 fermentation with the MemStir. Taken together, the results of the batch cultivations using MemStir show that bubble-free aeration for rhamnolipid production without oxygen limitation, foam formation, and the addition of antifoaming agent is possible.

3.4 | Process intensification by a tailored fed-batch strategy

To increase the rhamnolipid titer, fed-batch fermentations with both strains were conducted with a DO-based, thus C-limited feeding strategy to minimize oxygen consumption.

3.4.1 | KT2440 SK4 chassis in fed-batch mode

The DO-based fed-batch fermentation was conducted in biological duplicates with *P. putida* KT2440 SK4. For feeding a concentrated MSM with 200 g L^{-1} glucose was used. The fermentation started with a batch phase, which ended after glucose depletion at 9 h. After glucose depletion, the DO increased to 70%, and the feed phase was initiated (Figure 9b). In total, 46.3 g of glucose was fed within 12 h (corresponding to 20.7 g L^{-1}). At the end of the fermentation, 5.8 g rhamnolipids (2.6 g L^{-1}) and 14.1 g CDW (6.3 g L^{-1}) were reached (Figure 9a). The production of rhamnolipids and CDW followed a linear trend that can be explained by the C-limited fed-batch. Also, the ammonium sulfate increased linearly during the fed-batch, which means that only the carbon was limiting. After 12.5 h, the MemStir was operated at 100% pure oxygen to supply sufficient oxygen for *P. putida* KT2440 SK4. During aeration with 100% oxygen, the DO oscillated between 12% and 125% during each feed event. The feed solution increased the cultivation volume by 231 mL during the fed-batch operation, also taking into consideration the removed sample volume and the added volume of pH adjustment agent. At the same time, the membrane area remained the same. Consequently, the total oxygen transfer rate of the system continuously decreased over the fermentation time. For this reason, the high-peak DO decreased to 105% while the low peak did not drop below 10%. Thus, the

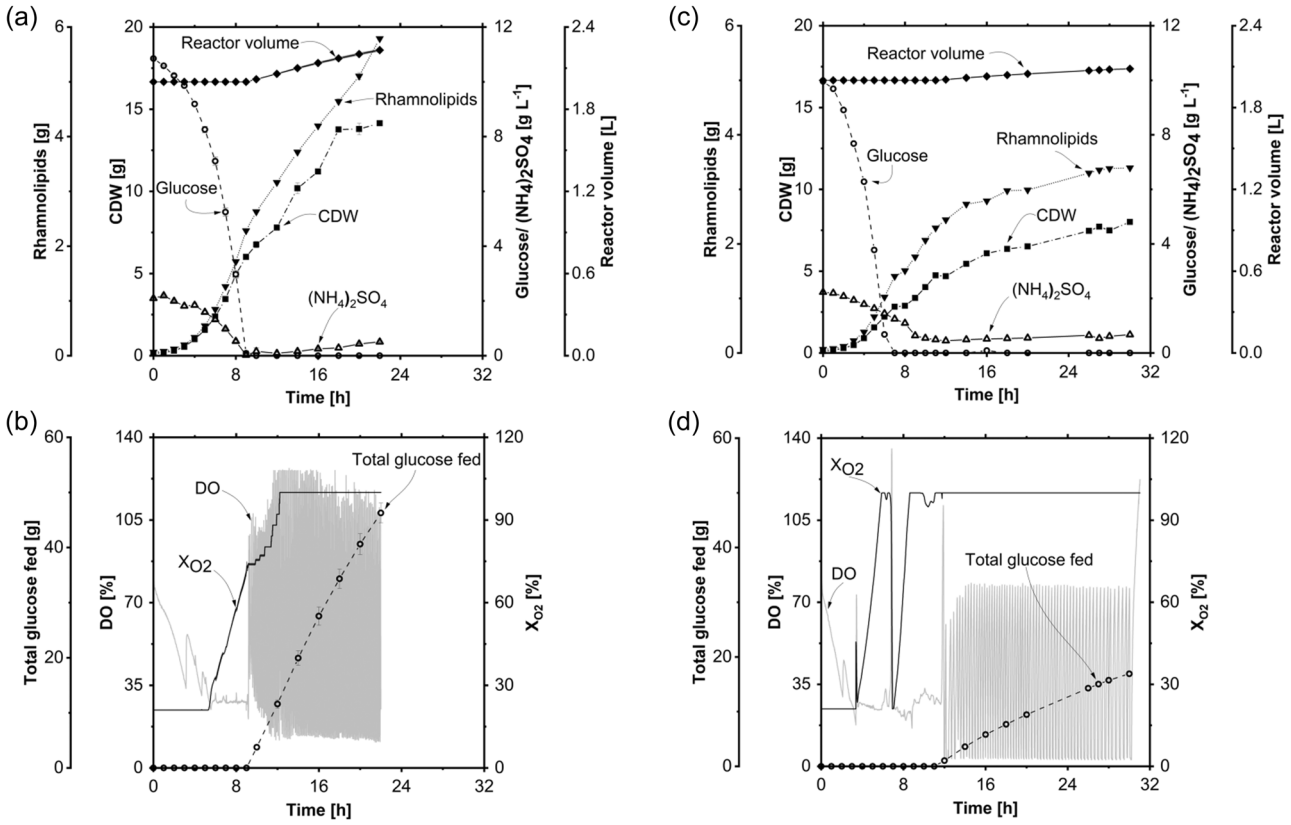

FIGURE 9 MemStir fed-batch fermentations with *P. putida* KT2440 SK4 (a and b) and *P. putida* KT2440 Δflag SK4 (c and d). The fed-batch cultivations were initially conducted in MSM using 10 g L^{-1} glucose at 30°C at pH 7 and inoculated with an OD_{600} of 0.2 (Section 2.6). For DO-based feeding, a highly concentrated MSM with 200 g L^{-1} glucose was used (Section 2.3). The feeding pump was activated when the DO signal increased, indicating a carbon source depletion. At a DO of 70%, the pump rate was set to 48 mL h^{-1} resulting in an addition of feed solution and a decrease of the DO. At a DO of 60%, feeding was stopped until the carbon source was again depleted, and 70% was reached. The total reactor volume was 3.3 L. The cultivation volume was 2.0 L, the aeration rate was 1.0 L min^{-1}, the stirring rate was between 100 and 300 min^{-1}, and the TMP was between 0 and 350 mbar (Section 2.6). (a) Trends of rhamnolipid, CDW, glucose, and $(NH_4)_2SO_4$ amounts/concentrations and the cultivation volume using *P. putida* KT2440 SK4. (b) Corresponding online signals of DO, X_{O2} and the total amount of glucose fed to graph (a). (c) Courses of rhamnolipid, CDW, glucose, and $(NH_4)_2SO_4$ amounts/concentrations and the reactor volume using *P. putida* KT2440 Δflag SK4. (d) Corresponding online signals of DO, X_{O2} and the total amount of glucose fed to graph (c). The error bars and error bands show the minimum and maximum values of two individual cultivations. CDW, cell-dry weight; DO, dissolved oxygen; TMP, transmembrane pressure.

cultivation was fully oxygenated for the entire period. If the cultivation volume increases, then the overall performance of the MemStir decreases as more and more volume needs to be supplied with oxygen. This means that the oscillation of the DO becomes smaller and smaller, especially in the high-peak. Since the total oxygen transfer decreased with increasing cultivation volume at constant membrane area, and the feed protocol fed reduced volumes per feed event towards the end of the cultivation, causing less feed solution to be fed. After 18 h, *P. putida* KT2440 SK4 stopped growing probably due to low trace element amounts supplied, as glucose was consumed throughout the process and ammonium sulfate and phosphate were present in sufficient amounts in the feed (Figure 9a). The amount of trace elements in the feed could not be increased since higher concentrations caused the feed medium to precipitate. Compared with the batch fermentation with the SK4 strain, the rhamnolipid titer (2.6 g L^{-1}) was increased by 2.2-fold. Furthermore, a STY of 118 mg_{RL} L^{-1} h^{-1} was achieved, equaling to the batch fermentation. With this setup, a $Y_{P/S}$ of 0.08 g_{RL} g_{Glc}^{-1} was reached, which is 0.7-fold lower than the batch fermentation (Table 1). This is probably since more carbon was used for biomass formation in the fed-batch process. The yield in the fed-batch process could be further improved by different feeding strategies (e.g., linear, exponential, or a combination of exponential and linear increasing). In addition, the feed composition could also be optimized to eliminate the potential limitation(s) of the process after 18 h.

3.5 | Energy-efficient chassis underperforms in intensified fermentation

The energy-saving strain was shown to outperform the SK4 strain in batch fermentation (Section 3.3.1 & 3.3.2). It was thus expected that

TABLE 1 Summary of studies producing rhamnolipids using bioreactor systems.

Organism	Process strategy	C-source	Time [h]	V_L [L]	CDW [g L^{-1}]	$\mu_{max,batch}$ [h^{-1}]	c_{RL} [g L^{-1}]	STY [mg $L^{-1}h^{-1}$]	$Y_{P/S}$ [g g^{-1}]	V_{AF} [mL]	Reference
P. putida KT2440 Δ flag SK4	Batch with AF addition	10 g L^{-1} glucose	10	1.20	3.12	0.46	0.33	36	0.04	27.9	This study
P. putida KT2440	Batch with MemStir	10 g L^{-1} glucose	10	2	2.57	0.59	1.17	118	0.11	-	""
SK4 *P. putida* KT2440 Δ flag SK4	Batch with MemStir	10 g L^{-1} glucose	11	2.00	2.49	0.61	1.37	124	0.13	-	""
P. putida KT2440 SK4	Fed-batch with MemStir	200 g L^{-1} glucose feed	22	2.23	6.34	0.55	2.59	118	0.08	-	""
P. putida KT2440 Δ flag SK4	Fed-batch with MemStir	200 g L^{-1} glucose feed	30	2.08	3.84	0.55	1.63	54	0.09	-	""
P. putida KT2440 SK4	Batch submerged membrane-module	10 g L^{-1} glucose	12	2.30	3.2	0.48	0.86	86	0.11	-	Bongartz et al. (2021)
P. putida KT2440 SK4	Fed-batch submerged membrane-module	750 g L^{-1} glucose feed	32	2.05	8.7	0.48	2.23	67	0.10	-	Bongartz et al. (2021)
P. putida Δ flag KT2440 SK4	Batch with foam recirculation	10 g L^{-1} glucose	10	1.0	2.8	0.56	1.50	160	0.13	-	Tiso et al. (2020)
P. putida KT2440 SK4	Batch with *in situ* extraction at pH = 6	10 g L^{-1} glucose	11	0.80	-	0.37	0.92	84	0.09	-	Demling et al. (2020)
P. aeruginosa PA1	Batch with external membrane-aeration	30 g L^{-1} glycerol	168	3.00	2.5	-	6.00	30	0.20	-	de Kronemberger et al. (2007)
P. putida EM383+pPS05 *rhlAB*	Fed-Batch with integrated foam adsorption	700 g L^{-1} glucose feed	82	2.60	5.5	-	6.00	73	0.05	-	Anic et al. (2018)
P. putida KT2440+pSynPro8oT *rhlAB*	Fed-Batch with AF addition	400 g L^{-1} glucose feed	72	1.50	23.5	0.44	14.70	204	0.09	≫ 20.0	Beuker et al. (2016)

Abbreviations: CDW, cell-dry weight; c_{RL}, final concentration of rhamnolipids; STY, space-time yield; $\mu_{max,batch}$, maximum growth rate in the batch phase; $Y_{P/S}$, rhamnolipid yield per substrate; V_{AF}, the added volume of antifoaming agent.

in the intensified setup, the productivity would increase even more. Therefore, DO-based fed-batch fermentation was performed. It is important to mention that the performance of the MemStir was expected to be lower in this fermentation since the membrane had already been used three times (Figure 4b). The fermentation started with a batch phase, which finished after 2-KG depletion at 11.8 h (see Figure S3B). After 7 h, the glucose was depleted, and 6.4 g L^{-1} 2-KG were accumulated in the culture broth (Figure S3B). This diauxic growth behavior was already observed in batch fermentation. As previously described, the MemStir had a decreased OTR_{max}, therefore, the oxygen content in the supply air was already at 100% during the batch phase (Figure 9d). This is twice as high compared to the previous batch fermentation. After 2-KG depletion, the DO reached 70%, and the feed phase was initiated. In total, 16.9 g glucose was fed within 18 h (corresponds to 8.1 g L^{-1}), which is 0.3-fold lower compared to the SK4 fed-batch fermentation. Noticeably, during the fed-batch phase, both CDW and rhamnolipid amounts increased from 4.7 g to only 8.0 g (3.8 g L^{-1}) and from 2.3 g to only 3.4 g (1.6 g L^{-1}), respectively (Figure 9c). This unexpected low increase may be due to three reasons. First, it could be due to the lower MemStir performance, as the DO repeatedly dropped below 10%. Thus, the organism was repetitively oxygen-limited for short periods. This may lead to slower metabolism, which could explain the slow increase in CDW and rhamnolipid amounts. Second, the deletion of the flagellum might have affected the carbon flux through the cell. A rearrangement of metabolic fluxes was visible before when the energy-saving strain accumulated 12-fold more 2-KG in the supernatant than *P. putida* KT2440 SK4 (Figure S3A,B). A third reason could be that the glucose concentration per feed event was too low since the half-velocity constant K_s for glucose uptake for *P. putida* KT2440 is approximately 0.2 g L^{-1} (Beuker et al., 2016). Therefore, the glucose concentration should be above the K_s value. If the concentration is below the K_s value, the rate slowed down, assuming Monod kinetics (Monod, 2012). With this setup and energy-saving strain *P. putida* KT2440 Δflag SK4, a $Y_{P/S}$ of 0.09 g_{RL} g_{Glc}^{-1} was reached, which is in the same range as in the SK4 fed-batch fermentation. However, the process time is 8 h longer, and the final rhamnolipid titer (1.6 g L^{-1}) is 0.6-fold lower compared to the *P. putida* KT2440 SK4 fed-batch cultivation (Table 1). The fermentation was terminated after 30 h, as hardly any growth could be detected anymore. The glucose was still consumed but probably oxidized to carbon dioxide and was no longer used for biomass or rhamnolipid production. This is also reflected in the STY, which is only half at 54 mg_{RL} L^{-1} h^{-1} for the energy-saving strain.

3.6 | State-of-the-art rhamnolipid yield reached by foam-free fermentation

The major results of the described fermentations are summarized and compared to published fermentations (Table 1). The strictly aerobic bacterium, *P. putida* KT2440, could be supplied with sufficient amounts of oxygen, which is a significant improvement to the previously reported static membrane module by Bongartz et al. (2021). In addition to the improvement in OTR_{max} to the static module, all further fermentation performance parameters were improved as well. Thus, the μ_{max} is 1.2-fold higher with the MemStir. Furthermore, the rhamnolipid titer is also 1.4-fold higher and, accordingly, the STY. The flagellar machinery has been shown to require a significant amount of metabolic energy. Elimination of this gene cluster could free up resources that can be used to synthesize rhamnolipids (Martínez- García et al., 2014; Tiso et al., 2020). This work also showed that using the energy-saving strain led to higher yields and titers than the SK4 strain in batch fermentations. In another study, a rhamnolipid titer of 0.92 g L^{-1} was achieved with 10 g L^{-1} glucose with *P. putida* KT2440 SK4 using in situ liquid–liquid extraction for the prevention of foam formation at a reduced pH value, which is 0.8-fold lower compared to our results (Demling et al., 2020). One reason for the lower rhamnolipid titer could be the lower pH value during the in situ extraction fermentation. Another study shows a membrane process for rhamnolipid production with an external membrane-aeration module and the opportunistic human pathogen *P. aeruginosa*. After 168 h of cultivation with 30 g L^{-1} glycerol, a rhamnolipid titer of 6 g L^{-1} was achieved, corresponding to a STY of 30 mg_{RL} L^{-1} h^{-1} (de Kronemberger et al., 2007). In our batch fermentations, less carbon was used, and the process time is 17-fold shorter. Thus, although the rhamnolipid titer is lower, the STY is 4.1-fold higher in this study. Furthermore, rhamnolipids were produced in this study using a recombinant *P. putida* KT2440 strain that is non-pathogenic (Kampers et al., 2019), which makes the process safer. The fed-batch process with *P. putida* KT2440 SK4 was improved compared with the previously reported static membrane module by Bongartz et al. (2021). The process was not oxygen-limited, and the processing time was reduced from 32 h to 22 h, thus the STY is increased 1.8-fold. Compared to previous reports about recombinant rhamnolipid production with *P. putida* KT2440, the obtained results here are comparable or even superior. In the SK4 fed-batch fermentation, a $Y_{P/S}$ of 0.08 g_{RL} g_{Glc}^{-1} and a STY of 118 mg_{RL} L^{-1} h^{-1} were reached (Table 1). In a study with an integrated rhamnolipid adsorption system using glucose as a carbon source, a $Y_{P/S}$ of 0.05 g_{RL} g_{Glc}^{-1} and a STY of 73 mg_{RL} L^{-1} h^{-1} were reached (Anic et al., 2018). Beuker et al. (2016) reported the so far highest recombinant produced rhamnolipid titer of 14.9 g L^{-1}, which corresponds to a $Y_{P/S}$ of 0.09 g_{RL} g_{Glc}^{-1} and a STY of 200 mg_{RL} L^{-1} h^{-1} in a fed-batch fermentation using 250 g glucose and more than 15 g L^{-1} antifoaming agent to control foaming. In summary, bubble-free aeration with the MemStir is a relevant innovation in bioreactor aeration technology. For the production of rhamnolipids, the MemStir has substantial advantages over conventional bubble-aerated systems or other bioreactor systems such as foam fractionation or in situ extraction. In conventional bubble aerated systems, the main problem is the foam formation and the addition of antifoaming agents, which leads to more difficult downstream processing of the product. With foam fractionation, cultivation conditions are more dynamic since there is an external loop through the foam fractionation column in which the organism tends to be exposed to limitations. For efficient foam fractionation, the loss of biocatalyst from the reactor due to biomass accumulation in the foam is a challenge (Blesken, Bator, et al., 2020). In addition, upscaling of

foam fractionation processes is complex as many parameters need to be considered. Also, in in situ extraction, a second organic phase is added to the reactor, changing the cultivation conditions. Furthermore, a very complex screening of solvents has to be carried out to avoid toxic effects and explosive atmospheres, especially on a larger scale (Demling et al., 2020). In membrane aeration, the growth conditions are usually the same as in bubble-aerated processes, with the difference that there is no foaming. Furthermore, no antifoaming agent is required, making subsequent downstream processing considerably less complex and cost-intensive. Performance loss of the MemStir after the initial process could be handled by two strategies: 1. in a single-use approach, especially for cell-cultivation in expensive biopharmaceutical processes, where the global trend points in all process units for disposable solutions (GMI, 2020). 2. Further investigation of a purification protocol may include washing detergent and protein-digesting enzymes. A scale-up, transfer to other bioreactors and transfer into an industrial application could then be achieved by the digital-twin construction- and simulation approach, already presented in Bongartz et al. (2021). One potential scale-up design could be a stack of stirrer modules with a wider diameter on top of each other. Also, bioprocesses in biopharmacy with comparable lower volumes to those in "white biotechnology" could profit from the shear stress-reduced aeration technology presented here. One major challenge for the upscale will be the exponential volume increase versus the linear increase of membrane-surface area. This could limit potential fields of applications to processes with a comparably low gas demand.

4 | CONCLUSION AND OUTLOOK

We report the construction and characterization of a flow-optimized submerged membrane-module stirrer (MemStir). The MemStir geometry is designed by CFD simulations for homogeneous mixing and maximum oxygen supply. Thus, the MemStir enables oxygen transfer efficiencies unreached by other membrane aeration systems (OTR_{max} of 175 mmol L^{-1} h^{-1}) into the bioreactor under given stirring conditions. Foam-preventing applications of the aeration platform were shown by comparative bubble-free cultivation of two rhamnolipid-producing *P. putida* strains in batch and fed-batch mode. A direct comparison with a bubble-aerated cultivation was made, and a more than 3-fold higher rhamnolipid concentration was achieved. In the MemStir aerated fermentations, we reached a STY up to 124 mg_{RL} L^{-1} h^{-1}. This STY is almost identical to published state-of-the-art fermentation approaches for recombinant rhamnolipid synthesis but, in contrast to conventional processes, renounced completely on bubble aeration and antifoaming agents. Beyond rhamnolipid production, this work discusses the applicability of the presented MemStir for the cultivation of vulnerable cells like animal cells. The CFD results indicate physiological flow conditions and oxygen supply with reduced harm to those cells. Cultivation with further organisms should be performed to expose the MemStir as a versatile bubble-free aeration platform technology. Of particular interest for biopharmaceutical production would be processes including animal cells.

AUTHOR CONTRIBUTION

Patrick Bongartz: Conceptualization; data curation; investigation; methodology; writing – original draft; writing – review & editing; visualization; validation, funding acquisition. **Tobias Karmainski**: Conceptualization; data curation; investigation; methodology; writing – original draft; writing – review & editing; visualization; validation. **Moritz Meyer**: Investigation; visualization. **John Linkhorst**: Methodology; validation; writing – review & editing; visualization; funding acquisition. **Till Tiso**: Methodology; validation; writing – review & editing; funding acquisition. **Lars Mathias Blank**: Methodology; validation; writing – review & editing; supervision; funding acquisition. **Matthias Wessling**: Conceptualization; writing – review & editing; supervision; funding acquisition; project administration.

ACKNOWLEDGMENTS

Prototypes of the modules were financed by the Innovation Sprint of the RWTH Aachen Innovation by the "Excellence Start-up Center.NRW" initiative, funded by the state of North Rhine-Westphalia. The sponsor is the Ministry of Economy, Innovation, Digitization and Energy. Simulations were performed with computing resources granted by RWTH Aachen University under project thes0610. Furthermore, the authors thank Robin Fröhlingsdorf, Christian Reich, Matthias Hesselmann (simulation), Alexander Scheele (design), Karin Faensen (FESEM), and Fabian Speen (fermentations) for their valuable input and many fruitful discussions. The laboratories of Matthias Wessling and Lars M. Blank have been partially funded by the Deutsche Forschungsgemeinschaft (DFG, German Research Foundation) under Germany's Excellence Strategy—Exzellenzcluster 2186 The Fuel Science Center" ID: 390919832. This work was also funded by the Bundesministerium für Bildung und Forschung (BMBF, GlycoX project, grant no. 161B0866B). Open Access funding enabled and organized by Projekt DEAL.

CONFLICT OF INTEREST STATEMENT

Patrick Bongartz, Moritz Meyer, and Matthias Wessling declare that they are inventors of a related pending patent (P. Bongartz, M. Meyer, M. Wessling; "INTEGRAL GAS-INTRODUCTION AND STIRRING UNIT FOR GAS-LIQUID REACTORS", RWTH Aachen University, 2021, WO2021152128 A1). Lars Mathias Blank and Till Tiso declare that they are inventors of three related patents. 1) L. M. Blank, F. Rosenau, S. Wilhelm, A. Wittgens, T. Tiso, "Means and methods for rhamnolipid production", HHU Dusseldorf University, TU Dortmund University, 2013 (WO 2013/041670 A1), 2) L. M. Blank, B. Küpper, E. M. del Amor Villa, R. Wichmann, C. Nowacki, "Foam adsorption", TU Dortmund University, 2013 (WO 2013/087674 A1), and 3) L. M. Blank, T. Tiso, A. Germer, "Extracellular production of designer hydroxyalkanoyloxy alkanoic acids with recombinant bacteria", RWTH Aachen University, 2015 (WO2017006252A1). We wish to confirm that there are no known other conflicts of interest associated with this publication.

DATA AVAILABILITY STATEMENT

The data that support the findings of this study are available from the corresponding author upon reasonable request.

ORCID

Patrick Bongartz https://orcid.org/0000-0002-2240-2671
Tobias Karmainski https://orcid.org/0000-0001-6589-2626
John Linkhorst https://orcid.org/0000-0002-8556-9217
Till Tiso http://orcid.org/0000-0003-4420-5609
Lars M. Blank https://orcid.org/0000-0003-0961-4976
Matthias Wessling http://orcid.org/0000-0002-7874-5315

REFERENCES

Abdel-Mawgoud, A. M., Lépine, F., & Déziel, E. (2010). Rhamnolipids: Diversity of structures, microbial origins and roles. *Applied Microbiology and Biotechnology*, *86*(5), 1323–1336.

Allen, S. M., Fujii, M., Stannett, V., Hopfenberg, H. B., & Williams, J. L. (1977). The barrier properties of polyacrylonitrile. *Journal of Membrane Science*, *2*, 153–163. https://doi.org/10.1016/S0376-7388(00)83241-X

Anic, I., Apolonia, I., Franco, P., & Wichmann, R. (2018). Production of rhamnolipids by integrated foam adsorption in a bioreactor system. *AMB Express*, *8*(1), 122. https://doi.org/10.1186/s13568-018-0651-y

Bator, I., Karmainski, T., Tiso, T., & Blank, L. M. (2020). Killing two birds with one stone – strain engineering facilitates the development of a unique rhamnolipid production process. *Frontiers in Bioengineering and Biotechnology*, *8*, 899.

Behrens, B., Baune, M., Jungkeit, J., Tiso, T., Blank, L. M., & Hayen, H. (2016). High performance liquid chromatography- charged aerosol detection applying an inverse gradient for quantification of rhamnolipid biosurfactants. *Journal of Chromatography A*, *1455*, 125–132. https://doi.org/10.1016/j.chroma.2016.05.079

Beuker, J., Barth, T., Steier, A., Wittgens, A., Rosenau, F., Henkel, M., & Hausmann, R. (2016). High titer heterologous rhamnolipid production. *AMB Express*, *6*(1), 124.

Blank, L. M., Ebert, B. E., Buehler, K., & Bühler, B. (2010). Redox biocatalysis and metabolism: Molecular mechanisms and metabolic network analysis. *Antioxidants & Redox Signaling*, *13*(3), 349–394. https://doi.org/10.1089/ars.2009.2931

Blank, L. M., Ionidis, G., Ebert, B. E., Bühler, B., & Schmid, A. (2008). Metabolic response of *Pseudomonas putida* during redox biocatalysis in the presence of a second octanol phase. *FEBS Journal*, *275*(20), 5173–5190.

Blesken, C. C., Bator, I., Eberlein, C., Heipieper, H. J., Tiso, T., & Blank, L. M. (2020). Genetic cell-surface modification for optimized foam fractionation. *Frontiers in Bioengineering and Biotechnology*, *8*. https://doi.org/10.3389/fbioe.2020.572892

Blesken, C. C., Strümpfler, T., Tiso, T., & Blank, L. M. (2020). Uncoupling foam fractionation and foam adsorption for enhanced biosurfactant synthesis and recovery. *Microorganisms*, *8*(12), 2029. https://doi.org/10.3390/microorganisms8122029

Bongartz, P., Bator, I., Baitalow, K., Keller, R., Tiso, T., Blank, L. M., & Wessling, M. (2021). A scalable bubble-free membrane aerator for biosurfactant production. *Biotechnology and Bioengineering*, *118*(9), 3545–3558. https://doi.org/10.1002/bit.27822

Brod, H., Kauling, J., Frahm, B., & Rose, R. (2009). Method and apparatus for the gassing and degassing of liquids, particularly in biotechnology, and specifically of cell cultures (US Patent App. 12/280,565).

Brown, A. K., Isbell, C., Gallagher, S., Dodd, P. W., & Varley, J. (2001). An improved method for controlling foams produced within bioreactors. *Food and Bioproducts Processing*, *79*(2), 114–121. https://doi.org/10.1205/096030801750286276

Carstensen, F., Apel, A., & Wessling, M. (2012). In situ product recovery: Submerged membranes vs. external loop mem branes. *Journal of Membrane Science*, *394-395*, 1–36.

Catapano, G. (2004). Turbulent flow technique for the estimation of oxygen diffusive permeability of membranes for the oxygenation of blood and other cell suspensions. *Journal of Membrane Science*, *230*(1-2), 131–139.

Chang, H. N., & Furusaki, S. (1991). Membrane bioreactors: Present and prospects. *Bioreactor Systems and Effects*, 27–64.

Charcosset, C. (2012). *Membrane processes in biotechnology and pharmaceutics*. Elsevier. https://doi.org/10.1016/C2011-0-04261-8

Chisti, Y. (2000). Animal-cell damage in sparged bioreactors. *Trends in Biotechnology*, *18*(10), 420–432.

Cote, P., Bersillon, J.-L., Huyard, A., & Faup, G. (1988). Bubble-free aeration using membranes: Process analysis. *Journal (Water Pollution Control Federation)*, 1986–1992.

Coutte, F., Lecouturier, D., Ait Yahia, S., Leclère, V., Béchet, M., Jacques, P., & Dhulster, P. (2010). Production of surfactin and fengycin by *Bacillus subtilis* in a bubbleless membrane bioreactor. *Applied Microbiology and Biotechnology*, *87*(2), 499–507. https://doi.org/10.1007/s00253-010-2504-8

Delvigne, F., & Lecomte, J.-P. (2010). Foam formation and control in bioreactors, *Encyclopedia of industrial biotechnology* (pp. 1–13). John Wiley & Sons, Ltd. https://doi.org/10.1002/9780470054581.eib326

Demling, P., Ankenbauer, A., Klein, B., Noack, S., Tiso, T., Takors, R., & Blank, L. M. (2021). *Pseudomonas putida* KT2440 endures temporary oxygen limitations. *Biotechnology and Bioengineering*, *118*(12), 4735–4750.

Demling, P., von Campenhausen, M., Grütering, C., Tiso, T., Jupke, A., & Blank, L. M. (2020). Selection of a recyclable *in situ* liquid–liquid extraction solvent for foam-free synthesis of rhamnolipids in a two-phase fermentation. *Green Chemistry*, *22*(23), 8495–8510. https://doi.org/10.1039/D0GC02885A

Djeljadini, S., Bongartz, P., Alders, M., Hartmann, N., Oing, A., Cornelissen, C., Hesselmann, F., Arens, J., Steinseifer, U., Linkhorst, J., & Wessling, M. (2021). Porous PVDF monoliths with templated geometry. *Advanced Materials Technologies*, *6*(11), 2100325. https://doi.org/10.1002/admt.202100325

Drioli, E., Curcio, E., & Di Profio, G. (2005). State of the art and recent progresses in membrane contactors. *Chemical Engineering Research and Design*, *83*(3), 223–233. https://doi.org/10.1205/cherd.04203

Ducommun, P., Ruffieux, P.-A., Furter, M.-P., Marison, I., & von Stockar, U. (2000). A new method for on-line measure- ment of the volumetric oxygen uptake rate in membrane aerated animal cell cultures. *Journal of Biotechnology*, *78*(2), 139–147.

Frahm, B., Brod, H., & Langer, U. (2009). Improving bioreactor cultivation conditions for sensitive cell lines by dynamic membrane aeration. *Cytotechnology*, *59*(1), 17–30.

Frahm, B., Kirchner, S., Kauling, J., Brod, H., Langer, U., & Bödeker, B. (2007). Dynamische membranbegasung im bioreaktor zur intensivierung der sauerstoffversorgung empfindlicher zelllinien. *Chemie Ingenieur Technik*, *79*(7), 1052–1058.

GMI. (2020). Bioreactors market size by product type (single use, reusable), by cell (mammalian cells, bacterial cells, yeast cells), by molecule (monoclonal antibodies, vaccines, recombinant proteins, stem cells, gene therapy), by usage (developmental, pre-clinical & clinical, commercial production), by end-use (R&D organizations, biopharma man-ufacturers, contract manufacturing organizations [cmos]), industry analysis, report, regional outlook, application potential, price trends, competitive market share & forecast 2021–2027. https://www.marketresearch.com/One-Off-Global-Market-Insights-v4130/Bioreactors-Size-Product-Type-Single-14273838

Guarino, R. D., Dike, L. E., Haq, T. A., Rowley, J. A., Pitner, J. B., & Timmins, M. R. (2004). Method for determining oxygen consumption rates of static cultures from microplate measurements of pericellular dissolved oxygen concentration. *Biotechnology and Bioengineering*, *86*(7), 775–787. https://doi.org/10.1002/bit.20072

Handa-Corrigan, A., Emery, A. N., & Spier, R. E. (1989). Effect of gas—liquid interfaces on the growth of suspended mammalian cells: Mechanisms of cell damage by bubbles. *Enzyme and Microbial Technology*, *11*(4), 230–235.

Hartmans, S., Bont, J. A. M., & Harder, W. (1989). Microbial metabolism of short-chain unsaturated hydrocarbons. *FEMS Microbiology Letters*, *63*(3), 235–264. https://doi.org/10.1016/0378-1097(89)90133-X

Heidemann, R., Riese, U., Lu¨tkemeyer, D., Bu¨ntemeyer, H., & Lehmann, J. (1994). The super-spinner: A low cost animal cell culture bioreactor for the CO_2 incubator. *Cytotechnology*, *14*(1), 1–9.

Henzler, H.-J. (2000). Particle stress in bioreactors. *Influence of stress on cell growth and product formation*, 35–82. In Springer. https://doi.org/10.1007/3-540-47865-5.

Jiang, J., Zu, Y., Li, X., Meng, Q., & Long, X. (2020). Recent progress towards industrial rhamnolipids fermentation: Process optimization and foam control. *Bioresource Technology*, *298*, 122394.

Junker, B. (2007). Foam and its mitigation in fermentation systems. *Biotechnology Progress*, *23*(4), 767–784.

Kampers, L. F. C., Volkers, R. J. M., & Martins dos Santos, V. A. P. (2019). *Pseudomonas putida* KT2440 is HV 1 certified, not GRAS. *Microbial Biotechnology*, *12*(5), 845–848.

Käß, F., Prasad, A., Tillack, J., Moch, M., Giese, H., Büchs, J., Wiechert, W., & Oldiges, M. (2014). Rapid assessment of oxygen transfer impact for *Corynebacterium glutamicum*. *Bioprocess and Biosystems Engineering*, *37*(12), 2567–2577.

Knazek, R. A., Gullino, P. M., Kohler, P. O., & Dedrick, R. L. (1972). Cell culture on artificial capillaries: An approach to tissue growth in vitro. *Science*, *178*(4056), 65–67.

de Kronemberger, F. A., Santa Anna, L. M. M., Fernandes, A. C. L. B., de Menezes, R. R., Borges, C. P., & Freire, D. M. G. (2007). Oxygen-controlled biosurfactant production in a bench scale bioreactor, *Biotechnology for fuels and chemicals* (pp. 401–413). In Springer. https://doi.org/10.1007/s12010-007-8057-3

Makagiansar, H. Y., Ayazi Shamlou, P., Thomas, C. R., & Lilly, M. D. (1993). The influence of mechanical forces on the morphol- ogy and penicillin production of *Penicillium chrysogenum*. *Bioprocess Engineering*, *9*(2), 83–90. https://doi.org/10.1007/BF00369035

Mandenius, C.-F. (2016). *Bioreactors: Design, operation and novel applications*. John Wiley & Sons.

Martínez- García, E., Nikel, P. I., Chavarría, M., & de Lorenzo, V. (2014). The metabolic cost of flagellar motion in *Pseu- domonas putida*. *Environmental Microbiology*, *16*(1), KT2440291–303.

Menniti, A., Kang, S., Elimelech, M., & Morgenroth, E. (2009). Influence of shear on the production of extracellular polymeric substances in membrane bioreactors. *Water Research*, *43*(17), 4305–4315.

Minamino, T., & Imada, K. (2015). The bacterial flagellar motor and its structural diversity. *Trends in Microbiology*, *23*(5), 267–274. https://doi.org/10.1016/j.tim.2014.12.011

Monod, J. (2012). The growth of bacterial cultures. *Selected Papers in Molecular Biology by Jacques Monod*, 139.

Nikel, P. I., Chavarría, M., Fuhrer, T., Sauer, U., & De Lorenzo, V. (2015). *Pseudomonas putida* KT2440 strain metabolizes glucose through a cycle formed by enzymes of the Entner-Doudoroff, Embden-Meyerhof-Parnas, and pentose phosphate pathways. *Journal of Biological Chemistry*, *290*(43), 25920–25932.

Palomares, L. A., & Ramírez, O. T. (2019). Hydrodynamic stress and heterogeneities in animal cell culture.

Qi, H. N., Goudar, C. T., Michaels, J. D., Henzler, H.-J., Jovanovic, G. N., & Konstantinov, K. B. (2003). Experimental and theoretical analysis of tubular membrane aeration for mammalian cell bioreactors. *Biotechnology Progress*, *19*(4), 1183–1189.

Routledge, S. J. (2012). Beyond de-foaming: The effects of antifoams on bioprocess productivity. *Computational and Structural Biotechnology Journal*, *3*(4), e201210001.

Santos-Moreau, V., Lopes, J. C. B., & Fonte, C. P. (2019). Estimation of kla values in bench-scale stirred tank reactors with self-inducing impeller by multiphase CFD simulations. *Chemical Engineering & Technology*, *42*(8), 1545–1554.

Schirmer, C., Blaschczok, K., Husemann, U., Leupold, M., Zahnow, C., Rupprecht, J., Glöckler, R., Greller, G., Pörtner, R., Eibl, R., & Eibl, D. (2017). Standardized qualification of stirred bioreactors for microbial biopharmaceutical production processes. *Chemie Ingenieur Technik*, *89*(12), 1766–1772. https://doi.org/10.1002/cite.201700039

Schlembach, I., Hosseinpour Tehrani, H., Blank, L. M., Büchs, J., Wierckx, N., Regestein, L., & Rosenbaum, M. A. (2020). Consolidated bioprocessing of cellulose to itaconic acid by a co-culture of *Trichoderma reesei* and *Ustilago maydis*. *Biotechnology for Biofuels*, *13*(1), 207. https://doi.org/10.1186/s13068-020-01835-4

Seidel, S., Maschke, R. W., Werner, S., Jossen, V., & Eibl, D. (2021). Oxygen mass transfer in biopharmaceutical processes: Numerical and experimental approaches. *Chemie Ingenieur Technik*, *93*(1–2), 42–61. https://doi.org/10.1002/cite.202000179

Sha, R., Meng, Q., & Jiang, L. (2012). The addition of ethanol as defoamer in fermentation of rhamnolipids. *Journal of Chemical Technology & Biotechnology*, *87*(3), 368–373.

Syron, E., & Casey, E. (2008). Membrane-aerated biofilms for high rate biotreatment: Performance appraisal, engineering principles, scale-up, and development requirements. *Environmental Science & Technology*, *42*(6), 1833–1844. https://doi.org/10.1021/es0719428

Tiso, T., Ihling, N., Kubicki, S., Biselli, A., Schonhoff, A., Bator, I., Thies, S., Karmainski, T., Kruth, S., Willenbrink, A.-L., Loeschcke, A., Zapp, P., Jupke, A., Jaeger, K. E., Büchs, J., & Blank, L. M. (2020). Integration of genetic and process engineering for optimized rhamnolipid production using *Pseudomonas putida*. *Frontiers in Bioengineering and Biotechnology*, *8*, 976. https://doi.org/10.3389/fbioe.2020.00976

Tiso, T., Zauter, R., Tulke, H., Leuchtle, B., Li, W.-J., Behrens, B., Wittgens, A., Rosenau, F., Hayen, H., & Blank, L. M. (2017). Designer rhamnolipids by reduction of congener diversity: Production and characterization. *Microbial Cell Factories*, *16*(1), 225. https://doi.org/10.1186/s12934-017-0838-y

Vardar-Sukan, F. (1998). Foaming: Consequences, prevention and destruction. *Biotechnology Advances*, *16*(5–6), 913–948.

Vorlop, J., & Lehmann, J. (1988). Scale-up of bioreactors for fermentation of mammalian cell cultures with special reference to oxygen supply and microcarrier mixing. *Chemical Engineering & Technology*, *11*(1), 171–178.

Wagner, B. A., Venkataraman, S., & Buettner, G. R. (2011). The rate of oxygen utilization by cells. *Free Radical Biology and Medicine*, *51*(3), 700–712. https://doi.org/10.1016/j.freeradbiomed.2011.05.024

Willis, R. B., Montgomery, M. E., & Allen, P. R. (1996). Improved method for manual, colorimetric determination of total Kjeldahl nitrogen using salicylate. *Journal of Agricultural and Food Chemistry*, *44*(7), 1804–1807.

Wittgens, A., Tiso, T., Arndt, T. T., Wenk, P., Hemmerich, J., Müller, C., Wichmann, R., Küpper, B., Zwick, M., Wil-helm, S., Hausmann, R., Syldatk, C., Rosenau, F., & Blank, L. M. (2011). Growth independent

rhamnolipid production from glucose using the non-pathogenic *Pseudomonas putida* KT2440. *Microbial Cell Factories*, *10*(1), 80. https://doi.org/10.1186/1475-2859-10-80

SUPPORTING INFORMATION

Additional supporting information can be found online in the Supporting Information section at the end of this article.

How to cite this article: Bongartz, P., Karmainski, T., Meyer, M., Linkhorst, J., Tiso, T., Blank, L. M., & Wessling, M. (2023). A novel membrane stirrer system enables foam-free biosurfactant production. *Biotechnology and Bioengineering*, 120, 1269–1287. https://doi.org/10.1002/bit.28334